Propagators and scattering of electromagnetic waves in planar bianisotropic slabs - an application to frequency selective structures

Kristensson, Gerhard; Poulsen, Sören; Rikte, Sten

2001

CODEN:LUTEDX/(TEAT-7099)/1-32/(2001)

Propagators and scattering of electromagnetic waves in planar bianisotropic slabs — an application to frequency selective structures

Gerhard Kristensson, Sören Poulsen, and Sten Rikte

Department of Electroscience
Electromagnetic Theory
Lund Institute of Technology
Sweden

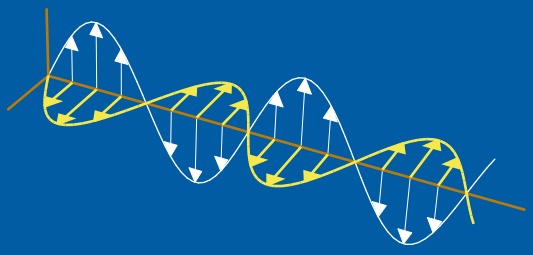

Gerhard Kristensson (Gerhard.Kristensson@es.lth.se)

Department of Electroscience
Electromagnetic Theory
Lund Institute of Technology
P.O. Box 118
SE-221 00 Lund
Sweden

Sören Poulsen (Soren.Poulsen@acab.se)

Applied Composites AB
P.O. Box 163
SE-341 23 Ljungby
Sweden

Sten Rikte (Sten.Rikte@kockums.se)

Kockums AB
SE-205 55 Malmö
Sweden

Editor: Gerhard Kristensson

Abstract

Scattering by planar geometries with plane metal inclusions are analyzed. The metal inclusions can be of arbitrary shape, and the material of the supporting slabs can be any linear (bianisotropic) material. We employ the method of propagators to find the solution of the scattering problem. The method has certain similarities with a vector generalization of the transmission line theory. A general relation between the electric fields and the surface current densities on the metal inclusions and the exciting fields are found. Special attention is paid to the case of a periodic metal pattern (frequency selective structures, FSS). The method is illustrated by a series of numerical computations.

1 Introduction

Wave propagation in planar geometries is a classical canonical scattering and radiation problem and many excellent papers and books treat this problem in great detail, see *e.g.*, [2, 8, 13, 19]. Any attempt to revisit this problem have to focus on a new systematic approach to solve the problem. This is exactly the reason and motivation of this paper. The concept of propagators that relates the total transverse fields to each other provides such a new concept. Moreover, it provides a systematic approach to analyze the solution of complicated scattering problems. The use of propagators in science is old, *e.g.*, in quantum mechanics [1], but seems to have been of little use in electromagnetic problems.

The work presented in this paper grew out of the analysis presented in [11] where an integral representation technique was applied. We present a novel approach — based on the concept of propagators — to solve scattering problems in planar geometries with an arbitrary number of metallic sheets imbedded in a slab. The method has certain similarities with a vector generalization of the transmission line theory [3, 16]. Specifically, the propagator technique is a vector generalization of the voltage-current transmission theory formulation [3] or transmission (ABCD) matrix [16].

The material in the supporting slabs can be arbitrary linear material, *i.e.*, a bianisotropic material. The integral representation approach presented in [11] can be generalized to treat also the more general case presented in this paper, but with an increasing complexity in the analysis. The proposed method with propagators makes considerable simplification in the analysis.

An important application of the theory presented in this paper is the case when the metallic scatterers are arranged in a periodic pattern. This is the frequency selective surface or structure case (FSS) and the theory and analysis of this application is thoroughly given in [14]. In the latter part of this paper the FSS geometry is analyzed and the advantages with the propagator approach become more transparent. The importance of dielectric layers in the design of a frequency selective surface is thoroughly treated in the excellent book of Munk [14].

The paper is organized in the following way: In Sections 2 and 3 the geometry and

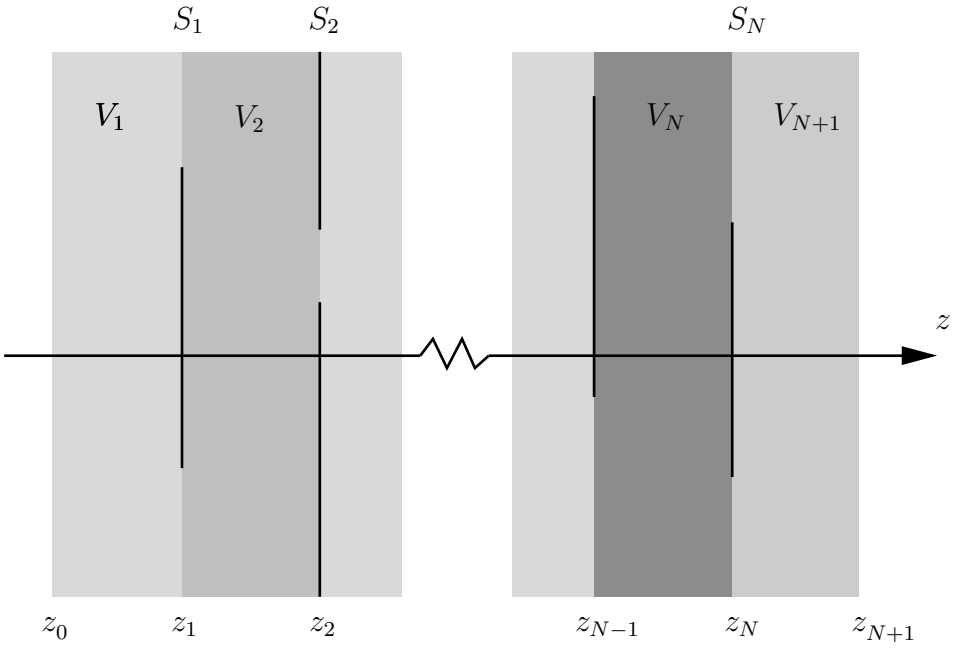

Figure 1: The geometry of the problem with patches or apertures at $z = z_1, \ldots, z_N$.

the prerequisites of the problem are presented. The propagators and the concept of wave splitting are presented in Section 4, and the general solution to the propagation problem is given in Section 5. The Galerkin's method is applied in Section 6. We specialize the analysis to the periodic case in Section 7 and give some numerical examples of the analysis in Section 8. An appendix with technical computations concludes the paper.

2 Geometry

The geometry of the problem analyzed in this paper is depicted in Figure 1. The depth parameter z is defined by the common normal of the indicated parallel interfaces. There are N thin, plane, metallic, perfectly conducting, scatterers (patches or apertures), $S_1, S_2, \ldots, S_N$, present, each of which is supported by a bianisotropic slab, *i.e.*, there are $N+1$ slabs, occupying the region $V_1, V_2, \ldots, V_{N+1}$. The locations of the thin scatterers are $z = z_n$, $n = 1, 2, \ldots, N$. The ends of the structure are represented by the coordinates z_0 and z_{N+1}. Thus, the location of the interfaces and the thin scatterers satisfies

$$z_0 < z_1 < z_2 < \cdots < z_{N-1} < z_N < z_{N+1}$$

We recall the time-harmonic ($e^{-i\omega t}$) constitutive relations of the general bian-

isotropic medium [17]:

$$\begin{cases} \boldsymbol{D} = \epsilon_0 \{\boldsymbol{\epsilon} \cdot \boldsymbol{E} + \eta_0 \boldsymbol{\xi} \cdot \boldsymbol{H}\} \\ \boldsymbol{B} = \dfrac{1}{c_0} \{\boldsymbol{\zeta} \cdot \boldsymbol{E} + \eta_0 \boldsymbol{\mu} \cdot \boldsymbol{H}\} \end{cases}$$

The permittivity and permeability of vacuum are denoted by ϵ_0 and μ_0, respectively. The speed of light in vacuum is $c_0 = 1/\sqrt{\epsilon_0 \mu_0}$ and the intrinsic impedance of vacuum is $\eta_0 = \sqrt{\mu_0/\epsilon_0}$. The bianisotropic slabs may have varying material dyadics $\boldsymbol{\epsilon}$, $\boldsymbol{\xi}$, $\boldsymbol{\zeta}$, $\boldsymbol{\mu}$, as functions of depth z (and angular frequency ω), *i.e.*, $\boldsymbol{\epsilon} = \boldsymbol{\epsilon}(z)$ *etc.* In particular, they can be homogeneous or stratified. In the lateral directions, x- and y-directions, there are no variations in the material parameters. The dynamics of the fields in the bianisotropic medium is modeled by the time-harmonic Maxwell equations in a source-free region:

$$\begin{cases} \nabla \times \boldsymbol{E} = ik_0 c_0 \boldsymbol{B} = ik_0 \{\boldsymbol{\zeta} \cdot \boldsymbol{E} + \eta_0 \boldsymbol{\mu} \cdot \boldsymbol{H}\} \\ \eta_0 \nabla \times \boldsymbol{H} = -ik_0 c_0 \eta_0 \boldsymbol{D} = -ik_0 \{\boldsymbol{\epsilon} \cdot \boldsymbol{E} + \eta_0 \boldsymbol{\xi} \cdot \boldsymbol{H}\} \end{cases} \tag{2.1}$$

where $k_0 = \omega/c_0$ is the vacuum wave number. The space outside the slabs is assumed to be vacuous, which covers all situation of interest in technical applications. The case of non-vacuous half spaces can be obtained as a limit process $z_0 \to -\infty$ and $z_{N+1} \to \infty$.

The sources of the problem are assumed to be confined to the regions (may be at infinity) located to the left or the right of all inhomogeneities, *i.e.*, they are contained in the vacuous half-spaces $z < z_0$ and $z > z_{N+1}$.

3 Lateral Fourier transform of the fields

With the geometry adopted in this paper, it is natural to decompose the fields in a spectrum of plane waves. The Fourier transform $\boldsymbol{E}(\boldsymbol{k}_t, z)$ of a time-harmonic field $\boldsymbol{E}(\boldsymbol{r})$, $\boldsymbol{r} = \hat{\boldsymbol{x}}x + \hat{\boldsymbol{y}}y + \hat{\boldsymbol{z}}z$, with respect to the lateral position vector $\boldsymbol{\rho} = \hat{\boldsymbol{x}}x + \hat{\boldsymbol{y}}y$ is defined by

$$\boldsymbol{E}(\boldsymbol{k}_t, z) = \iint_{-\infty}^{\infty} \boldsymbol{E}(\boldsymbol{r}) e^{-i\boldsymbol{k}_t \cdot \boldsymbol{\rho}} \, dx \, dy$$

where the real vector

$$\boldsymbol{k}_t = \hat{\boldsymbol{x}} k_x + \hat{\boldsymbol{y}} k_y$$

is the lateral wave vector and the non-negative (real) number

$$k_t = \sqrt{k_x^2 + k_y^2}$$

is the lateral wave number. By the Fourier inversion formula,

$$\boldsymbol{E}(\boldsymbol{r}) = \frac{1}{4\pi^2} \iint_{-\infty}^{\infty} \boldsymbol{E}(\boldsymbol{k}_t, z) e^{i\boldsymbol{k}_t \cdot \boldsymbol{\rho}} \, dk_x \, dk_y \tag{3.1}$$

Observe that only the argument of the field indicates whether the field itself $\boldsymbol{E}(\boldsymbol{r})$ or its Fourier transform $\boldsymbol{E}(\boldsymbol{k}_t, z)$ w.r.t. $\boldsymbol{\rho}$ is intended, and that the (real) unit vectors[1]

$$\begin{cases} \hat{\boldsymbol{e}}_{\parallel}(\boldsymbol{k}_t) = \boldsymbol{k}_t/k_t \\ \hat{\boldsymbol{e}}_{\perp}(\boldsymbol{k}_t) = \hat{\boldsymbol{z}} \times \hat{\boldsymbol{e}}_{\parallel}(\boldsymbol{k}_t) \end{cases}$$

constitute a orthogonal basis for the lateral vectors (vectors in the x-y-plane).

3.1 Consequences for the Maxwell equations

As a consequence of lateral Fourier transformation of the electric and magnetic fields, the Maxwell equations (2.1) for the bianisotropic medium are transformed into the system of six coupled ordinary differential equations (ODE)

$$\begin{cases} \dfrac{\mathrm{d}}{\mathrm{d}z}\mathbf{J} \cdot \boldsymbol{E}(\boldsymbol{k}_t, z) + i\boldsymbol{k}_t \times \boldsymbol{E}(\boldsymbol{k}_t, z) = ik_0 \left\{ \boldsymbol{\zeta}(z) \cdot \boldsymbol{E}(\boldsymbol{k}_t, z) + \boldsymbol{\mu}(z) \cdot \eta_0 \boldsymbol{H}(\boldsymbol{k}_t, z) \right\} \\ \dfrac{\mathrm{d}}{\mathrm{d}z}\mathbf{J} \cdot \eta_0 \boldsymbol{H}(\boldsymbol{k}_t, z) + i\boldsymbol{k}_t \times \eta_0 \boldsymbol{H}(\boldsymbol{k}_t, z) = -ik_0 \left\{ \boldsymbol{\epsilon}(z) \cdot \boldsymbol{E}(\boldsymbol{k}_t, z) + \boldsymbol{\xi}(z) \cdot \eta_0 \boldsymbol{H}(\boldsymbol{k}_t, z) \right\} \end{cases}$$

where the dyadic $\mathbf{J} = \hat{\boldsymbol{z}} \times \mathbf{I}_2$ represents a projection in the x-y-plane and a rotation of $\pi/2$ around the z-axis.

By utilizing the unique decomposition of the fields in their lateral components, $\boldsymbol{E}_{xy}(\boldsymbol{k}_t, z)$ and $\eta_0 \boldsymbol{H}_{xy}(\boldsymbol{k}_t, z)$, and their corresponding longitudinal (z) components, $E_z(\boldsymbol{k}_t, z)$ and $\eta_0 H_z(\boldsymbol{k}_t, z)$, *i.e.*,

$$\begin{cases} \boldsymbol{E}(\boldsymbol{k}_t, z) = \boldsymbol{E}_{xy}(\boldsymbol{k}_t, z) + \hat{\boldsymbol{z}} E_z(\boldsymbol{k}_t, z) \\ \boldsymbol{H}(\boldsymbol{k}_t, z) = \boldsymbol{H}_{xy}(\boldsymbol{k}_t, z) + \hat{\boldsymbol{z}} H_z(\boldsymbol{k}_t, z) \end{cases}$$

and by introducing these decompositions in the Maxwell equations, it follows that the longitudinal field components can be eliminated. A system of ODE:s for the lateral fields, the fundamental equation for one-dimensional time-harmonic wave propagation in bianisotropic materials [17], remains:

$$\frac{\mathrm{d}}{\mathrm{d}z} \begin{pmatrix} \boldsymbol{E}_{xy}(\boldsymbol{k}_t, z) \\ \hat{\boldsymbol{z}} \times \eta_0 \boldsymbol{H}_{xy}(\boldsymbol{k}_t, z) \end{pmatrix} = ik_0 \mathbf{M}(\boldsymbol{k}_t, z) \cdot \begin{pmatrix} \boldsymbol{E}_{xy}(\boldsymbol{k}_t, z) \\ \hat{\boldsymbol{z}} \times \eta_0 \boldsymbol{H}_{xy}(\boldsymbol{k}_t, z) \end{pmatrix} \tag{3.2}$$

where the linear map $\mathbf{M}(\boldsymbol{k}_t, z)\colon \mathbb{C}^2 \times \mathbb{C}^2 \to \mathbb{C}^2 \times \mathbb{C}^2$ depends on the material dyadics. A detailed representation of $\mathbf{M}(\boldsymbol{k}_t, z)$ in terms of $\boldsymbol{\epsilon}(z)$, $\boldsymbol{\xi}(z)$, $\boldsymbol{\zeta}(z)$, $\boldsymbol{\mu}(z)$, $\boldsymbol{k}_t$, and k_0 is given in [17]. In homogeneous regions, the map $\mathbf{M}(\boldsymbol{k}_t, z)$ is independent of z, *i.e.*, $\mathbf{M}(\boldsymbol{k}_t, z) = \mathbf{M}(\boldsymbol{k}_t)$. Specifically, in vacuum, $\mathbf{M}(\boldsymbol{k}_t)$ is given by[2]

$$\mathbf{M}_0(\boldsymbol{k}_t) = \begin{pmatrix} \mathbf{0} & -\mathbf{I}_2 + \frac{1}{k_0^2}\boldsymbol{k}_t\boldsymbol{k}_t \\ -\mathbf{I}_2 - \frac{1}{k_0^2}\boldsymbol{k}_t \times (\boldsymbol{k}_t \times \mathbf{I}_2) & \mathbf{0} \end{pmatrix} \tag{3.3}$$

[1] The definition is meaningful only when $k_t \neq 0$. When $k_t = 0$, we choose $\hat{\boldsymbol{e}}_{\parallel} = \hat{\boldsymbol{x}}$ and $\hat{\boldsymbol{e}}_{\perp} = \hat{\boldsymbol{y}}$.

[2] The map $\mathbf{M}_0(\boldsymbol{k}_t)$ can be represented in a number of ways due to the identities $\boldsymbol{k}_t \times (\boldsymbol{k}_t \times \mathbf{I}_2) = \boldsymbol{k}_t\boldsymbol{k}_t - k_t^2\mathbf{I}_2$ and $k_t^2 + k_z^2 = k_0^2$.

where the identity dyadic in $\mathbb{R}^2$ for lateral vectors $\mathbf{I}_2 = \hat{\boldsymbol{e}}_\parallel\hat{\boldsymbol{e}}_\parallel + \hat{\boldsymbol{e}}_\perp\hat{\boldsymbol{e}}_\perp$ has been introduced. In view of the form of (3.2), it is also convenient to introduce the dyadic $\mathbf{J} = \hat{\boldsymbol{z}} \times \mathbf{I}_2$ that represents a rotation of $\pi/2$ around the z-axis. One has $\mathbf{J} = \hat{\boldsymbol{e}}_\perp\hat{\boldsymbol{e}}_\parallel - \hat{\boldsymbol{e}}_\parallel\hat{\boldsymbol{e}}_\perp$.

The eigenvalues of the vacuum quantity $k_0\mathbf{M}_0(\boldsymbol{k}_t)$ defined in (3.3) are found to be[3] k_z, k_z, $-k_z$, and $-k_z$, where the longitudinal wave number k_z is

$$k_z = \left(k_0^2 - k_t^2\right)^{1/2} = \begin{cases} \sqrt{k_0^2 - k_t^2} \text{ for } k_t < k_0 \\ i\sqrt{k_t^2 - k_0^2} \text{ for } k_t > k_0 \end{cases} \tag{3.4}$$

and the standard convention of the square root of a non-negative argument is intended. Consequently, k_z is a real non-negative number for propagating waves and a purely imaginary number with non-negative imaginary part for evanescent waves. Thus, for plane waves in vacuum regions, the general solution is of the form

$$\begin{cases} \boldsymbol{E}(\boldsymbol{k}_t, z) = \boldsymbol{E}^+(\boldsymbol{k}_t)e^{ik_z z} + \boldsymbol{E}^-(\boldsymbol{k}_t)e^{-ik_z z} \\ \boldsymbol{H}(\boldsymbol{k}_t, z) = \boldsymbol{H}^+(\boldsymbol{k}_t)e^{ik_z z} + \boldsymbol{H}^-(\boldsymbol{k}_t)e^{-ik_z z} \end{cases} \tag{3.5}$$

where $\boldsymbol{E}^\pm(\boldsymbol{k}_t)$ and $\boldsymbol{H}^\pm(\boldsymbol{k}_t)$ are constant, complex vectors.

4 Propagation in the stratified region

The wave propagator concept for the total transformed lateral electromagnetic field proved almost indispensable in [17]. The propagator maps the transformed lateral fields at z to another position z'. Formally we write

$$\begin{pmatrix} \boldsymbol{E}_{xy}(\boldsymbol{k}_t, z) \\ \eta_0\mathbf{J} \cdot \boldsymbol{H}_{xy}(\boldsymbol{k}_t, z) \end{pmatrix} = \mathbf{P}(\boldsymbol{k}_t, z, z') \cdot \begin{pmatrix} \boldsymbol{E}_{xy}(\boldsymbol{k}_t, z') \\ \eta_0\mathbf{J} \cdot \boldsymbol{H}_{xy}(\boldsymbol{k}_t, z') \end{pmatrix} \tag{4.1}$$

This formulation is a vector generalization of the voltage-current transmission theory formulation [3] or transmission (ABCD) matrix [16]. The propagator satisfy the same system of ODE:s as the lateral fields (3.2), *i.e.*,

$$\begin{cases} \dfrac{\mathrm{d}}{\mathrm{d}z}\mathbf{P}(\boldsymbol{k}_t, z, z') = ik_0\mathbf{M}(\boldsymbol{k}_t, z) \cdot \mathbf{P}(\boldsymbol{k}_t, z, z') \\ \mathbf{P}(\boldsymbol{k}_t, z', z') = \mathbf{I}_4 \end{cases}$$

[3]The determinant of a (square) matrix with square diagonal blocks is

$$\det \begin{pmatrix} \mathbf{A}_{11} & \mathbf{A}_{12} \\ \mathbf{A}_{21} & \mathbf{A}_{22} \end{pmatrix} = \det\left(\mathbf{A}_{11} \cdot \mathbf{A}_{22} - \mathbf{A}_{12} \cdot \mathbf{A}_{22}^{-1} \cdot \mathbf{A}_{21} \cdot \mathbf{A}_{22}\right),$$

provided that $\mathbf{A}_{22}$ is non-singular. Therefore,

$$\det(\lambda\mathbf{I}_4 - k_0\mathbf{M}_0(\boldsymbol{k}_t)) = \det(\mathbf{I}_2(\lambda^2 - (k_0^2 - k_t^2))) = (\lambda^2 - k_z^2)^2 = (\lambda - k_z)^2(\lambda + k_z)^2$$

The augmented initial condition when both z-arguments of the propagator $\mathbf{P}$ coincide is due to the fact that the lateral fields at z then are mapped onto themselves, *i.e.*, the identity mapping $\mathbf{I}_4$ in $\mathbb{C}^4$.

Several examples of explicit expressions of the propagators are found in [17]. Specifically, the propagator for vacuum is [17]

$$\mathbf{P}_0(\boldsymbol{k}_t, z, z') = e^{ik_0(z-z')\mathbf{M}_0(\boldsymbol{k}_t)} = \mathbf{I}_4 \cos k_z(z-z') + \frac{ik_0}{k_z}\mathbf{M}_0(\boldsymbol{k}_t) \sin k_z(z-z') \quad (4.2)$$

where the longitudinal wave number k_z is given by (3.4). This propagator can be written as a spectral decomposition

$$\mathbf{P}_0(\boldsymbol{k}_t, z, z') = \mathbf{Q}^+(\boldsymbol{k}_t)e^{ik_z(z-z')} + \mathbf{Q}^-(\boldsymbol{k}_t)e^{-ik_z(z-z')} \quad (4.3)$$

where the spectral projections

$$\begin{aligned}\mathbf{Q}^{\pm}(\boldsymbol{k}_t) =& \frac{1}{2}\left(\mathbf{I}_4 \pm \frac{k_0}{k_z}\mathbf{M}_0(\boldsymbol{k}_t)\right) = \frac{1}{2}\begin{pmatrix} \mathbf{I}_2 & \mp\mathbf{W}(\boldsymbol{k}_t) \\ \mp\mathbf{W}^{-1}(\boldsymbol{k}_t) & \mathbf{I}_2 \end{pmatrix} \\ =& \frac{1}{2}\begin{pmatrix} \mathbf{I}_2 & \mp\frac{k_0}{k_z}\left(\mathbf{I}_2 - \frac{1}{k_0^2}\boldsymbol{k}_t\boldsymbol{k}_t\right) \\ \mp\frac{k_0}{k_z}\left(\mathbf{I}_2 + \frac{1}{k_0^2}\boldsymbol{k}_t \times (\boldsymbol{k}_t \times \mathbf{I}_2)\right) & \mathbf{I}_2 \end{pmatrix}\end{aligned}$$

satisfy the relations

$$\begin{cases} \mathbf{Q}^{\pm}(\boldsymbol{k}_t) \cdot \mathbf{Q}^{\pm}(\boldsymbol{k}_t) = \mathbf{Q}^{\pm}(\boldsymbol{k}_t) \\ \mathbf{Q}^{\mp}(\boldsymbol{k}_t) \cdot \mathbf{Q}^{\pm}(\boldsymbol{k}_t) = \mathbf{0} \\ \mathbf{Q}^{+}(\boldsymbol{k}_t) + \mathbf{Q}^{-}(\boldsymbol{k}_t) = \mathbf{I}_2 \\ \mathbf{Q}^{+}(\boldsymbol{k}_t) - \mathbf{Q}^{-}(\boldsymbol{k}_t) = \dfrac{k_0}{k_z}\mathbf{M}_0(\boldsymbol{k}_t) \end{cases}$$

Substituting (4.3) into (4.1) gives the vacuum solution

$$\begin{aligned}\begin{pmatrix} \boldsymbol{E}_{xy}(\boldsymbol{k}_t, z) \\ \eta_0\mathbf{J} \cdot \boldsymbol{H}_{xy}(\boldsymbol{k}_t, z) \end{pmatrix} =& e^{ik_z(z-z')}\mathbf{Q}^+(\boldsymbol{k}_t) \cdot \begin{pmatrix} \boldsymbol{E}_{xy}(\boldsymbol{k}_t, z') \\ \eta_0\mathbf{J} \cdot \boldsymbol{H}_{xy}(\boldsymbol{k}_t, z') \end{pmatrix} \\ &+ e^{-ik_z(z-z')}\mathbf{Q}^-(\boldsymbol{k}_t) \cdot \begin{pmatrix} \boldsymbol{E}_{xy}(\boldsymbol{k}_t, z') \\ \eta_0\mathbf{J} \cdot \boldsymbol{H}_{xy}(\boldsymbol{k}_t, z') \end{pmatrix}\end{aligned} \quad (4.4)$$

in concordance with (3.5). Equation (4.4) can be regarded as the foundation of the concept of wave splitting in vacuum regions, to be presented in the next section.

4.1 Wave splitting

We introduce a wave-splitting technique that decomposes any Fourier transformed field into two components that transport power in the $+z$- or the $-z$-directions, respectively. An alternative characterization of the wave splitting transformation is that this transformation projects out the incident and reflected (transmitted) fields

out of the total field. The wave-splitting technique in vacuum is presented in detail in *e.g.*, [17]. We have

$$\begin{pmatrix} \boldsymbol{E}_{xy}(\boldsymbol{k}_t, z) \\ \eta_0 \mathbf{J} \cdot \boldsymbol{H}_{xy}(\boldsymbol{k}_t, z) \end{pmatrix} = \begin{pmatrix} \mathbf{I}_2 & \mathbf{I}_2 \\ -\mathbf{W}^{-1}(\boldsymbol{k}_t) & \mathbf{W}^{-1}(\boldsymbol{k}_t) \end{pmatrix} \cdot \begin{pmatrix} \boldsymbol{F}^+(\boldsymbol{k}_t, z) \\ \boldsymbol{F}^-(\boldsymbol{k}_t, z) \end{pmatrix} \tag{4.5}$$

where[4]

$$\mathbf{W}^{-1}(\boldsymbol{k}_t) = \frac{k_0}{k_z} \left(\mathbf{I}_2 + \frac{1}{k_0^2} \boldsymbol{k}_t \times (\boldsymbol{k}_t \times \mathbf{I}_2) \right) = \hat{\boldsymbol{e}}_\parallel \hat{\boldsymbol{e}}_\parallel \frac{k_0}{k_z} + \hat{\boldsymbol{e}}_\perp \hat{\boldsymbol{e}}_\perp \frac{k_z}{k_0} \tag{4.6}$$

where, as above, $\mathbf{I}_2$ is the identity dyadic in the x-y-plane. The inverse of this dyadic in the x-y-plane is

$$\begin{aligned} \mathbf{W}(\boldsymbol{k}_t) =& \frac{k_z}{k_0} \left(\mathbf{I}_2 - \frac{1}{k_z^2} \boldsymbol{k}_t \times (\boldsymbol{k}_t \times \mathbf{I}_2) \right) = \hat{\boldsymbol{e}}_\parallel \hat{\boldsymbol{e}}_\parallel \frac{k_z}{k_0} + \hat{\boldsymbol{e}}_\perp \hat{\boldsymbol{e}}_\perp \frac{k_0}{k_z} \\ =& \frac{k_0}{k_z} \left(\mathbf{I}_2 - \frac{1}{k_0^2} \boldsymbol{k}_t \boldsymbol{k}_t \right) = \frac{k_0}{k_z} \mathbf{I}_2 - \frac{k_t^2}{k_0 k_z} \hat{\boldsymbol{e}}_\parallel \hat{\boldsymbol{e}}_\parallel \end{aligned}$$

and we have

$$\begin{pmatrix} \boldsymbol{F}^+(\boldsymbol{k}_t, z) \\ \boldsymbol{F}^-(\boldsymbol{k}_t, z) \end{pmatrix} = \frac{1}{2} \begin{pmatrix} \mathbf{I}_2 & -\mathbf{W}(\boldsymbol{k}_t) \\ \mathbf{I}_2 & \mathbf{W}(\boldsymbol{k}_t) \end{pmatrix} \cdot \begin{pmatrix} \boldsymbol{E}_{xy}(\boldsymbol{k}_t, z) \\ \eta_0 \mathbf{J} \cdot \boldsymbol{H}_{xy}(\boldsymbol{k}_t, z) \end{pmatrix} \tag{4.7}$$

cf. equation (4.4).

To see the physical implications of this transformation, we proceed by finding the PDE for the split fields $\boldsymbol{F}^\pm$ in vacuum. The transverse fields $\boldsymbol{E}_{xy}(\boldsymbol{k}_t, z)$ and $\boldsymbol{H}_{xy}(\boldsymbol{k}_t, z)$ satisfy, see (3.2) and (3.3)

$$\frac{\mathrm{d}}{\mathrm{d}z} \begin{pmatrix} \boldsymbol{E}_{xy}(\boldsymbol{k}_t, z) \\ \mathbf{J} \cdot \eta_0 \boldsymbol{H}_{xy}(\boldsymbol{k}_t, z) \end{pmatrix} = ik_z \begin{pmatrix} \mathbf{0} & -\mathbf{W}(\boldsymbol{k}_t) \\ -\mathbf{W}^{-1}(\boldsymbol{k}_t) & \mathbf{0} \end{pmatrix} \cdot \begin{pmatrix} \boldsymbol{E}_{xy}(\boldsymbol{k}_t, z) \\ \mathbf{J} \cdot \eta_0 \boldsymbol{H}_{xy}(\boldsymbol{k}_t, z) \end{pmatrix}$$

since

$$\begin{cases} \mathbf{I}_2 - \dfrac{1}{k_0^2} \boldsymbol{k}_t \boldsymbol{k}_t = \dfrac{k_z}{k_0} \mathbf{W}(\boldsymbol{k}_t) \\ \mathbf{I}_2 + \dfrac{1}{k_0^2} \boldsymbol{k}_t \times (\boldsymbol{k}_t \times \mathbf{I}_2) = \dfrac{k_z}{k_0} \mathbf{W}^{-1}(\boldsymbol{k}_t) \end{cases}$$

An application of (4.5) and (4.7) gives

$$\frac{\mathrm{d}}{\mathrm{d}z} \begin{pmatrix} \boldsymbol{F}^+(\boldsymbol{k}_t, z) \\ \boldsymbol{F}^-(\boldsymbol{k}_t, z) \end{pmatrix} = ik_z \begin{pmatrix} \mathbf{I}_2 & \mathbf{0} \\ \mathbf{0} & -\mathbf{I}_2 \end{pmatrix} \cdot \begin{pmatrix} \boldsymbol{F}^+(\boldsymbol{k}_t, z) \\ \boldsymbol{F}^-(\boldsymbol{k}_t, z) \end{pmatrix}$$

[4]This dyadic is related to the admittance dyadic $\mathbf{Y}(\boldsymbol{k}_t)$.

$$\mathbf{Y}(\boldsymbol{k}_t) = \frac{1}{k_0 k_z} \left\{ k_0^2 \hat{\boldsymbol{e}}_\perp \hat{\boldsymbol{e}}_\parallel - k_z^2 \hat{\boldsymbol{e}}_\parallel \hat{\boldsymbol{e}}_\perp \right\} = \mathbf{J} \cdot \mathbf{W}^{-1}(\boldsymbol{k}_t)$$

From this equation we see that the split fields $\boldsymbol{F}^{\pm}$ decouple in vacuum and the solution is

$$\boldsymbol{F}^{\pm}(\boldsymbol{k}_t, z) = \boldsymbol{F}^{\pm}(\boldsymbol{k}_t, z_0) e^{\pm i k_z (z - z_0)}$$

Moreover, the contribution of the split fields $\boldsymbol{F}^{\pm}$ to the power flow (Poynting's vector), averaged over a plane $z =$ constant is [11, 17]

$$\frac{1}{2}\hat{\boldsymbol{z}} \cdot \mathrm{Re} \iint_{-\infty}^{\infty} \boldsymbol{E}(\boldsymbol{r}) \times \boldsymbol{H}(\boldsymbol{r})^* \, dx \, dy = \pm \frac{1}{8\pi^2 \eta \eta_0} \iint_{k_t \leq k} \frac{k_z}{k} \left| \boldsymbol{\gamma}^{\pm}(\boldsymbol{k}_t) \cdot \boldsymbol{F}^{\pm}(\boldsymbol{k}_t, z) \right|^2 \, dk_x \, dk_y$$

for the two split fields, respectively. The dyadics $\boldsymbol{\gamma}^{\pm}$ are defined in (7.8).

4.2 Propagators

The notion of propagator, defined in (4.1), is a very powerful tool for the analysis of wave propagation for a geometry as depicted Figure 1. In each of the bianisotropic regions we have ($n = 0, \cdots, N$)

$$\begin{pmatrix} \boldsymbol{E}_{xy}(\boldsymbol{k}_t, z_n^+) \\ \eta_0 \mathbf{J} \cdot \boldsymbol{H}_{xy}(\boldsymbol{k}_t, z_n^+) \end{pmatrix} = \mathbf{P}(\boldsymbol{k}_t, z_n, z_{n+1}) \cdot \begin{pmatrix} \boldsymbol{E}_{xy}(\boldsymbol{k}_t, z_{n+1}^-) \\ \eta_0 \mathbf{J} \cdot \boldsymbol{H}_{xy}(\boldsymbol{k}_t, z_{n+1}^-) \end{pmatrix} \tag{4.8}$$

where the wave propagator

$$\mathbf{P}(\boldsymbol{k}_t, z_n, z_{n+1}) = \begin{pmatrix} \mathbf{P}_{ee}(\boldsymbol{k}_t, z_n, z_{n+1}) & \mathbf{P}_{em}(\boldsymbol{k}_t, z_n, z_{n+1}) \\ \mathbf{P}_{me}(\boldsymbol{k}_t, z_n, z_{n+1}) & \mathbf{P}_{mm}(\boldsymbol{k}_t, z_n, z_{n+1}) \end{pmatrix}$$

for the general linear medium was presented in [17]. Similarly, for the two vacuous half spaces

$$\begin{pmatrix} \boldsymbol{E}_{xy}(\boldsymbol{k}_t, z) \\ \eta_0 \mathbf{J} \cdot \boldsymbol{H}_{xy}(\boldsymbol{k}_t, z) \end{pmatrix} = \mathbf{P}(\boldsymbol{k}_t, z, z_0) \cdot \begin{pmatrix} \boldsymbol{E}_{xy}(\boldsymbol{k}_t, z_0) \\ \eta_0 \mathbf{J} \cdot \boldsymbol{H}_{xy}(\boldsymbol{k}_t, z_0) \end{pmatrix}, \qquad z < z_0 \tag{4.9}$$

$$\begin{pmatrix} \boldsymbol{E}_{xy}(\boldsymbol{k}_t, z) \\ \eta_0 \mathbf{J} \cdot \boldsymbol{H}_{xy}(\boldsymbol{k}_t, z) \end{pmatrix} = \mathbf{P}(\boldsymbol{k}_t, z, z_{N+1}) \cdot \begin{pmatrix} \boldsymbol{E}_{xy}(\boldsymbol{k}_t, z_{N+1}) \\ \eta_0 \mathbf{J} \cdot \boldsymbol{H}_{xy}(\boldsymbol{k}_t, z_{N+1}) \end{pmatrix}, \qquad z > z_{N+1} \tag{4.10}$$

where the propagators are given explicitly by (4.2).

In the following section these relations between the transverse fields at different z-coordinates are exploited more in detail, and their use to solve the wave propagation problem becomes clear.

5 General formulation of problem

We are now in a position of combining the results of the previous sections together. The main concepts in the context are the notion of propagators, *i.e.*, the equations in Section 4.2, and the wave splitting concept presented in Section 4.1. The latter concept makes the necessary decomposition of the fields outside the slabs in order to identify the correct input and output components of the field.

Since the longitudinal components of the fields have been eliminated, and only the transverse components remain, the boundary conditions imply that the field quantities, $\boldsymbol{E}_{xy}(\boldsymbol{k}_t, z)$ and $\eta_0 \boldsymbol{H}_{xy}(\boldsymbol{k}_t, z)$, are continuous in z over any non-metallic interface. Moreover, at the thin, metallic sheets the electric field $\boldsymbol{E}_{xy}(\boldsymbol{k}_t, z_n)$ is continuous in z, since it is zero from both sides at the metallic parts, *i.e.*, zero at z_n^+ and at z_n^-, and continuous in z everywhere outside the metallic parts. However, the magnetic field $\boldsymbol{H}_{xy}(\boldsymbol{k}_t, z_n)$ has a jump discontinuity in z due to the presence of the induced surface currents on the metal parts. The total induced current distributions (sum from both sides) on the N different screens are

$$\boldsymbol{J}_S(\boldsymbol{k}_t, z_n) = \mathbf{J} \cdot \boldsymbol{H}_{xy}(\boldsymbol{k}_t, z_n^+) - \mathbf{J} \cdot \boldsymbol{H}_{xy}(\boldsymbol{k}_t, z_n^-), \qquad n = 1, \cdots, N \tag{5.1}$$

where, as above, the dyadic $\mathbf{J} = \hat{\boldsymbol{z}} \times \mathbf{I}_2$.

Equation (4.8) is now used to relate the fields at different z-positions. We apply (4.8) directly to the the internal slabs, *i.e.*, for $n = 1, \cdots, N-1$. The exterior slabs, *i.e.*, for $n = 0$ and $n = N$, is next to a half space, and to identify the correct input and output parts of the fields, we first apply the wave splitting transformation, (4.7). This is necessary in order to identify the pertinent reflection and transmission quantities of the entire slab and its metal scatterer. The result of the wave splitting transformation is

$$\begin{aligned} &\begin{pmatrix} \boldsymbol{F}^+(\boldsymbol{k}_t, z_0) \\ \boldsymbol{F}^-(\boldsymbol{k}_t, z_0) \end{pmatrix} \\ =&\frac{1}{2} \begin{pmatrix} \mathbf{P}_{ee} - \mathbf{W} \cdot \mathbf{P}_{me} & \mathbf{P}_{em} - \mathbf{W} \cdot \mathbf{P}_{mm} \\ \mathbf{P}_{ee} + \mathbf{W} \cdot \mathbf{P}_{me} & \mathbf{P}_{em} + \mathbf{W} \cdot \mathbf{P}_{mm} \end{pmatrix} (\boldsymbol{k}_t, z_0, z_1) \cdot \begin{pmatrix} \boldsymbol{E}_{xy}(\boldsymbol{k}_t, z_1) \\ \eta_0 \mathbf{J} \cdot \boldsymbol{H}_{xy}(\boldsymbol{k}_t, z_1^-) \end{pmatrix} \end{aligned} \tag{5.2}$$

and

$$\begin{aligned} &\begin{pmatrix} \boldsymbol{F}^+(\boldsymbol{k}_t, z_{N+1}) \\ \boldsymbol{F}^-(\boldsymbol{k}_t, z_{N+1}) \end{pmatrix} \\ =&\frac{1}{2} \begin{pmatrix} \mathbf{P}_{ee} - \mathbf{W} \cdot \mathbf{P}_{me} & \mathbf{P}_{em} - \mathbf{W} \cdot \mathbf{P}_{mm} \\ \mathbf{P}_{ee} + \mathbf{W} \cdot \mathbf{P}_{me} & \mathbf{P}_{em} + \mathbf{W} \cdot \mathbf{P}_{mm} \end{pmatrix} (\boldsymbol{k}_t, z_{N+1}, z_N) \cdot \begin{pmatrix} \boldsymbol{E}_{xy}(\boldsymbol{k}_t, z_N) \\ \eta_0 \mathbf{J} \cdot \boldsymbol{H}_{xy}(\boldsymbol{k}_t, z_N^+) \end{pmatrix} \end{aligned} \tag{5.3}$$

where $\mathbf{W}$ is the vacuum wave splitting operator. In these expressions the incoming transverse fields from the left and the right hand side of the slab are $\boldsymbol{F}^+(\boldsymbol{k}_t, z_0)$ and $\boldsymbol{F}^-(\boldsymbol{k}_t, z_{N+1})$, respectively. Similarly, the scattered transverse fields in the half spaces are $\boldsymbol{F}^-(\boldsymbol{k}_t, z_0)$ and $\boldsymbol{F}^+(\boldsymbol{k}_t, z_{N+1})$, respectively.

To solve the propagation problem for the entire slab, we use equations (4.8), (5.2), and (5.3) to express the scattered fields, $\boldsymbol{F}^-(\boldsymbol{k}_t, z_0)$ and $\boldsymbol{F}^+(\boldsymbol{k}_t, z_{N+1})$, and

the doubly represented magnetic fields at the screens, $\boldsymbol{H}_{xy}(\boldsymbol{k}_t, z_n^{\pm})$, $n = 1, \cdots, N$, in terms of the incoming fields, $\boldsymbol{F}^{+}(\boldsymbol{k}_t, z_0)$ and $\boldsymbol{F}^{-}(\boldsymbol{k}_t, z_{N+1})$, and the electric fields at the screens, $\boldsymbol{E}_{xy}(\boldsymbol{k}_t, z_n)$, $n = 1, \cdots, N$ (note that the electric field is continuous at z_n and, therefore, it is irrelevant which side of the metallic scatterer the transverse electric field is evaluated). Finally, by equation (5.1), the current densities at the screens, $\boldsymbol{J}_S(\boldsymbol{k}_t, z_n)$, $n = 1, \cdots, N$, can be related to the electric fields at the screens, $\boldsymbol{E}_{xy}(\boldsymbol{k}_t, z_n)$, $n = 1, \cdots, N$.

To this end, we write equation (4.8) (for $n = 1, \cdots, N-1$) in the form[5]

$$\begin{aligned}
&\begin{pmatrix} \eta_0 \mathbf{J} \cdot \boldsymbol{H}_{xy}(\boldsymbol{k}_t, z_n^{+}) \\ \eta_0 \mathbf{J} \cdot \boldsymbol{H}_{xy}(\boldsymbol{k}_t, z_{n+1}^{-}) \end{pmatrix} \\
&= \begin{pmatrix} \mathbf{P}_{mm} \cdot \mathbf{P}_{em}^{-1} & \mathbf{P}_{me} - \mathbf{P}_{mm} \cdot \mathbf{P}_{em}^{-1} \cdot \mathbf{P}_{ee} \\ \mathbf{P}_{em}^{-1} & -\mathbf{P}_{em}^{-1} \cdot \mathbf{P}_{ee} \end{pmatrix} (\boldsymbol{k}_t, z_n, z_{n+1}) \cdot \begin{pmatrix} \boldsymbol{E}_{xy}(\boldsymbol{k}_t, z_n) \\ \boldsymbol{E}_{xy}(\boldsymbol{k}_t, z_{n+1}) \end{pmatrix}
\end{aligned}$$

Hence, using equation (5.1),

$$\begin{aligned}
\eta_0 \boldsymbol{J}_S(\boldsymbol{k}_t, z_n) =& \mathbf{A}_{nn-1}(\boldsymbol{k}_t) \cdot \boldsymbol{E}_{xy}(\boldsymbol{k}_t, z_{n-1}) \\
&+ \mathbf{A}_{nn}(\boldsymbol{k}_t) \cdot \boldsymbol{E}_{xy}(\boldsymbol{k}_t, z_n) \qquad (n = 2, \cdots, N-1) \\
&+ \mathbf{A}_{nn+1}(\boldsymbol{k}_t) \cdot \boldsymbol{E}_{xy}(\boldsymbol{k}_t, z_{n+1})
\end{aligned} \tag{5.4}$$

where[6]

$$\begin{cases}
\mathbf{A}_{nn-1}(\boldsymbol{k}_t) = -\mathbf{P}_{em}^{-1}(\boldsymbol{k}_t, z_{n-1}, z_n) \\
\mathbf{A}_{nn}(\boldsymbol{k}_t) = (\mathbf{P}_{mm} \cdot \mathbf{P}_{em}^{-1})(\boldsymbol{k}_t, z_n, z_{n+1}) + (\mathbf{P}_{em}^{-1} \cdot \mathbf{P}_{ee})(\boldsymbol{k}_t, z_{n-1}, z_n) \\
\mathbf{A}_{nn+1}(\boldsymbol{k}_t) = (\mathbf{P}_{me} - \mathbf{P}_{mm} \cdot \mathbf{P}_{em}^{-1} \cdot \mathbf{P}_{ee})(\boldsymbol{k}_t, z_n, z_{n+1})
\end{cases} \tag{5.5}$$

Equation (5.4) is a relation between the surface current at the interior screens and the transverse electric fields at the screen and at its two neighbors. Similarly, using (5.1), the relations between the transverse magnetic fields the exterior screens and the transverse electric fields at the screen and its closest neighbor are found to be

$$\begin{aligned}
&\eta_0 \mathbf{J} \cdot \boldsymbol{H}_{xy}(\boldsymbol{k}_t, z_1^{+}) \\
&= \begin{pmatrix} \mathbf{P}_{mm} \cdot \mathbf{P}_{em}^{-1} & \mathbf{P}_{me} - \mathbf{P}_{mm} \cdot \mathbf{P}_{em}^{-1} \cdot \mathbf{P}_{ee} \end{pmatrix} (\boldsymbol{k}_t, z_1, z_2) \cdot \begin{pmatrix} \boldsymbol{E}_{xy}(\boldsymbol{k}_t, z_1) \\ \boldsymbol{E}_{xy}(\boldsymbol{k}_t, z_2) \end{pmatrix}
\end{aligned} \tag{5.6}$$

and

$$\eta_0 \mathbf{J} \cdot \boldsymbol{H}_{xy}(\boldsymbol{k}_t, z_N^{-}) = \begin{pmatrix} \mathbf{P}_{em}^{-1} & -\mathbf{P}_{em}^{-1} \cdot \mathbf{P}_{ee} \end{pmatrix} (\boldsymbol{k}_t, z_{N-1}, z_N) \cdot \begin{pmatrix} \boldsymbol{E}_{xy}(\boldsymbol{k}_t, z_{N-1}) \\ \boldsymbol{E}_{xy}(\boldsymbol{k}_t, z_N) \end{pmatrix} \tag{5.7}$$

[5]The formula is written in an economical form, and the dependence on the parameters must be read with caution. For instance, $(\mathbf{P}_{mm} \cdot \mathbf{P}_{em}^{-1})(\boldsymbol{k}_t, z_n, z_{n+1})$ should be interpreted as $\mathbf{P}_{mm}(\boldsymbol{k}_t, z_n, z_{n+1}) \cdot \mathbf{P}_{em}^{-1}(\boldsymbol{k}_t, z_n, z_{n+1})$. This convention is used throughout this section.

[6]Here and in the following we suppress the dependence of the block matrices $\mathbf{A}_{mn}(\boldsymbol{k}_t)$ on the location of the screens.

On the other hand, the scattering relations (5.2) and (5.3) can be written as

$$\boldsymbol{F}^{-}(\boldsymbol{k}_t, z_0) = \mathbf{C}_0(\boldsymbol{k}_t) \cdot \boldsymbol{F}^{+}(\boldsymbol{k}_t, z_0) + \mathbf{C}_1(\boldsymbol{k}_t) \cdot \boldsymbol{E}_{xy}(\boldsymbol{k}_t, z_1) \tag{5.8}$$

where

$$\begin{cases} \mathbf{C}_0(\boldsymbol{k}_t) = \left((\mathbf{P}_{em} + \mathbf{W} \cdot \mathbf{P}_{mm}) \cdot (\mathbf{P}_{em} - \mathbf{W} \cdot \mathbf{P}_{mm})^{-1}\right)(\boldsymbol{k}_t, z_0, z_1) \\ \mathbf{C}_1(\boldsymbol{k}_t) = \Big(-\frac{1}{2}(\mathbf{P}_{em} + \mathbf{W} \cdot \mathbf{P}_{mm}) \cdot (\mathbf{P}_{em} - \mathbf{W} \cdot \mathbf{P}_{mm})^{-1} \cdot (\mathbf{P}_{ee} - \mathbf{W} \cdot \mathbf{P}_{me}) \\ \qquad\qquad +\frac{1}{2}(\mathbf{P}_{ee} + \mathbf{W} \cdot \mathbf{P}_{me})\Big)(\boldsymbol{k}_t, z_0, z_1) \end{cases} \tag{5.9}$$

This expression is a relation between the input field from the left, $\boldsymbol{F}^{+}(\boldsymbol{k}_t, z_0)$, and the (unknown) scattered field to the left, $\boldsymbol{F}^{-}(\boldsymbol{k}_t, z_0)$, which consists of both a reflected and a transmitted part, and the (unknown) electric field on the first scatterer, $\boldsymbol{E}_{xy}(\boldsymbol{k}_t, z_1)$. Similarly, at the other side of the entire slab we get

$$\boldsymbol{F}^{+}(\boldsymbol{k}_t, z_{N+1}) = \mathbf{D}_{N+1}(\boldsymbol{k}_t) \cdot \boldsymbol{F}^{-}(\boldsymbol{k}_t, z_{N+1}) + \mathbf{D}_N(\boldsymbol{k}_t) \cdot \boldsymbol{E}_{xy}(\boldsymbol{k}_t, z_N) \tag{5.10}$$

where

$$\begin{cases} \mathbf{D}_{N+1}(\boldsymbol{k}_t) = \left((\mathbf{P}_{em} - \mathbf{W} \cdot \mathbf{P}_{mm}) \cdot (\mathbf{P}_{em} + \mathbf{W} \cdot \mathbf{P}_{mm})^{-1}\right)(\boldsymbol{k}_t, z_{N+1}, z_N) \\ \mathbf{D}_N(\boldsymbol{k}_t) = \Big(-\frac{1}{2}(\mathbf{P}_{em} - \mathbf{W} \cdot \mathbf{P}_{mm}) \cdot (\mathbf{P}_{em} + \mathbf{W} \cdot \mathbf{P}_{mm})^{-1} \cdot (\mathbf{P}_{ee} + \mathbf{W} \cdot \mathbf{P}_{me}) \\ \qquad\qquad +\frac{1}{2}(\mathbf{P}_{ee} - \mathbf{W} \cdot \mathbf{P}_{me})\Big)(\boldsymbol{k}_t, z_{N+1}, z_N) \end{cases} \tag{5.11}$$

This expression is a relation between the input field from the right, $\boldsymbol{F}^{-}(\boldsymbol{k}_t, z_{N+1})$, and the (unknown) scattered field to the right, $\boldsymbol{F}^{+}(\boldsymbol{k}_t, z_{N+1})$, which consists of both a reflected and a transmitted part, and the (unknown) electric field on the last scatterer, $\boldsymbol{E}_{xy}(\boldsymbol{k}_t, z_N)$.

Moreover, from the relations (5.2) and (5.3) have the relations

$$\begin{aligned} &\eta_0 \mathbf{J} \cdot \boldsymbol{H}_{xy}(\boldsymbol{k}_t, z_1^{-}) = 2(\mathbf{P}_{em} - \mathbf{W} \cdot \mathbf{P}_{mm})^{-1}(\boldsymbol{k}_t, z_0, z_1) \cdot \boldsymbol{F}^{+}(\boldsymbol{k}_t, z_0) \\ &- ((\mathbf{P}_{em} - \mathbf{W} \cdot \mathbf{P}_{mm})^{-1} \cdot (\mathbf{P}_{ee} - \mathbf{W} \cdot \mathbf{P}_{me}))(\boldsymbol{k}_t, z_0, z_1) \cdot \boldsymbol{E}_{xy}(\boldsymbol{k}_t, z_1) \end{aligned} \tag{5.12}$$

and

$$\begin{aligned} &\eta_0 \mathbf{J} \cdot \boldsymbol{H}_{xy}(\boldsymbol{k}_t, z_N^{+}) = 2(\mathbf{P}_{em} + \mathbf{W} \cdot \mathbf{P}_{mm})^{-1}(\boldsymbol{k}_t, z_{N+1}, z_N) \cdot \boldsymbol{F}^{-}(\boldsymbol{k}_t, z_{N+1}) \\ &- ((\mathbf{P}_{em} + \mathbf{W} \cdot \mathbf{P}_{mm})^{-1} \cdot (\mathbf{P}_{ee} + \mathbf{W} \cdot \mathbf{P}_{me}))(\boldsymbol{k}_t, z_{N+1}, z_N) \cdot \boldsymbol{E}_{xy}(\boldsymbol{k}_t, z_N) \end{aligned} \tag{5.13}$$

at the exterior screens.

To proceed, we divide the analysis into two separate paths, depending on whether there are one screen ($N = 1$) or whether there are several ($N > 1$). These cases are different due to the fact that in the first case the screen has the two half spaces next to the screen. In the second case there is always a screen as a neighbor.

5.1 Special case — several screens ($N > 1$)

The goal of this section is to find the expression that relates the surface currents on the screens, $\boldsymbol{J}_S(\boldsymbol{k}_t, z_n)$, to the electric field on the screens, $\boldsymbol{E}_{xy}(\boldsymbol{k}_t, z_n)$, and to the excitations of the entire slab, $\boldsymbol{F}^+(\boldsymbol{k}_t, z_0)$ and $\boldsymbol{F}^-(\boldsymbol{k}_t, z_{N+1})$.

We express the surface current at the first screen by a combination of the equations (5.6) and (5.12). The result is

$$\begin{aligned}\eta_0 \boldsymbol{J}_S(\boldsymbol{k}_t, z_1) =& \mathbf{A}_{11}(\boldsymbol{k}_t) \cdot \boldsymbol{E}_{xy}(\boldsymbol{k}_t, z_1) + \mathbf{A}_{12}(\boldsymbol{k}_t) \cdot \boldsymbol{E}_{xy}(\boldsymbol{k}_t, z_2) \\ &+ \mathbf{A}_{10}(\boldsymbol{k}_t) \cdot \boldsymbol{F}^+(\boldsymbol{k}_t, z_0)\end{aligned} \tag{5.14}$$

where

$$\begin{cases} \mathbf{A}_{11}(\boldsymbol{k}_t) =& (\mathbf{P}_{mm} \cdot \mathbf{P}_{em}^{-1})(\boldsymbol{k}_t, z_1, z_2) \\ & + ((\mathbf{P}_{em} - \mathbf{W} \cdot \mathbf{P}_{mm})^{-1} \cdot (\mathbf{P}_{ee} - \mathbf{W} \cdot \mathbf{P}_{me}))(\boldsymbol{k}_t, z_0, z_1) \\ \mathbf{A}_{12}(\boldsymbol{k}_t) =& (\mathbf{P}_{me} - \mathbf{P}_{mm} \cdot \mathbf{P}_{em}^{-1} \cdot \mathbf{P}_{ee})(\boldsymbol{k}_t, z_1, z_2) \\ \boldsymbol{A}_{10}(\boldsymbol{k}_t) =& -2(\mathbf{P}_{em} - \mathbf{W} \cdot \mathbf{P}_{mm})^{-1}(\boldsymbol{k}_t, z_0, z_1) \end{cases}$$

By combining equations (5.7) and (5.13) we get the surface current at the last screen

$$\begin{aligned}\eta_0 \boldsymbol{J}_S(\boldsymbol{k}_t, z_N) =& \mathbf{A}_{NN-1}(\boldsymbol{k}_t) \cdot \boldsymbol{E}_{xy}(\boldsymbol{k}_t, z_{N-1}) + \mathbf{A}_{NN}(\boldsymbol{k}_t) \cdot \boldsymbol{E}_{xy}(\boldsymbol{k}_t, z_N) \\ &+ \mathbf{A}_{NN+1}(\boldsymbol{k}_t) \cdot \boldsymbol{F}^-(\boldsymbol{k}_t, z_{N+1})\end{aligned} \tag{5.15}$$

where

$$\begin{cases} \mathbf{A}_{NN-1}(\boldsymbol{k}_t) = -\mathbf{P}_{em}^{-1}(\boldsymbol{k}_t, z_{N-1}, z_N) \\ \mathbf{A}_{NN}(\boldsymbol{k}_t) = (\mathbf{P}_{em}^{-1} \cdot \mathbf{P}_{ee})(\boldsymbol{k}_t, z_{N-1}, z_N) \\ \qquad\qquad - ((\mathbf{P}_{em} + \mathbf{W} \cdot \mathbf{P}_{mm})^{-1} \cdot (\mathbf{P}_{ee} + \mathbf{W} \cdot \mathbf{P}_{me}))(\boldsymbol{k}_t, z_{N+1}, z_N) \\ \mathbf{A}_{NN+1}(\boldsymbol{k}_t) = 2(\mathbf{P}_{em} + \mathbf{W} \cdot \mathbf{P}_{mm})^{-1}(\boldsymbol{k}_t, z_{N+1}, z_N) \end{cases}$$

Equations (5.4), (5.14), and (5.15) constitutes a set of equations that can be combined into a single expression ($n = 1, \cdots, N$)

$$\begin{aligned}\eta_0 \boldsymbol{J}_S(\boldsymbol{k}_t, z_n) =& \sum_{m=1}^{N} \mathbf{A}_{nm}(\boldsymbol{k}_t) \cdot \boldsymbol{E}_{xy}(\boldsymbol{k}_t, z_m) \\ &+ \delta_{n1} \mathbf{A}_{10}(\boldsymbol{k}_t) \cdot \boldsymbol{F}^+(\boldsymbol{k}_t, z_0) + \delta_{nN} \mathbf{A}_{NN+1}(\boldsymbol{k}_t) \cdot \boldsymbol{F}^-(\boldsymbol{k}_t, z_{N+1})\end{aligned} \tag{5.16}$$

which is the starting point for the Galerkin procedure. Note that the sum in the expression above only has at most three terms, since all matrices $\mathbf{A}_{nm}$ vanish if $m \neq n, n \pm 1$. The equation (5.16) can be written in compact form by composing the square ($2N \times 2N$) matrix of band block type

$$\mathbf{A}(\boldsymbol{k}_t) = (\mathbf{A}_{nm}(\boldsymbol{k}_t))$$

from the square (2×2) matrices $\mathbf{A}_{nm}(\boldsymbol{k}_t)$, $m, n = 1, \cdots, N$, *i.e.*,

$$\mathbf{A} = \begin{pmatrix} \mathbf{A}_{11} & \mathbf{A}_{12} & \mathbf{0} & \dots & \dots & \dots \\ \mathbf{A}_{21} & \mathbf{A}_{22} & \mathbf{A}_{23} & \mathbf{0} & \dots & \dots \\ \mathbf{0} & \mathbf{A}_{32} & \mathbf{A}_{33} & \mathbf{A}_{34} & \mathbf{0} & \dots \\ \vdots & \vdots & \vdots & \ddots & \vdots & \vdots \\ \dots & \dots & \mathbf{0} & \mathbf{A}_{N-1N-2} & \mathbf{A}_{N-1N-1} & \mathbf{A}_{N-1N} \\ \dots & \dots & \dots & \mathbf{0} & \mathbf{A}_{NN-1} & \mathbf{A}_{NN} \end{pmatrix}$$

The simple block band characteristics of the matrix $\mathbf{A}(\boldsymbol{k}_t)$ have several advantages that is used below. Moreover, by introducing the inverse $\mathbf{B} = \mathbf{A}^{-1}$ of $\mathbf{A}$, which is not of band block type, and decomposing this matrix as

$$\mathbf{B}(\boldsymbol{k}_t) = (\mathbf{B}_{nm}(\boldsymbol{k}_t))$$

where the dimension of the block matrices $\mathbf{B}_{nm}(\boldsymbol{k}_t)$, $m, n = 1, \cdots, N$, is 2×2, equation (5.16) can be inverted and the transverse electric field $\boldsymbol{E}_{xy}(\boldsymbol{k}_t, z_n)$ can be found in terms of the surface currents $\boldsymbol{J}_S(\boldsymbol{k}_t, z_m)$:

$$\begin{aligned} \boldsymbol{E}_{xy}(\boldsymbol{k}_t, z_n) = &\sum_{m=1}^{N} \mathbf{B}_{nm}(\boldsymbol{k}_t) \cdot \eta_0 \boldsymbol{J}_S(\boldsymbol{k}_t, z_m) \\ &- \mathbf{B}_{n0}(\boldsymbol{k}_t) \cdot \boldsymbol{F}^{+}(\boldsymbol{k}_t, z_0) - \mathbf{B}_{nN+1}(\boldsymbol{k}_t) \cdot \boldsymbol{F}^{-}(\boldsymbol{k}_t, z_{N+1}) \end{aligned} \tag{5.17}$$

where $\mathbf{B}_{n0}(\boldsymbol{k}_t) := \mathbf{B}_{n1}(\boldsymbol{k}_t) \cdot \mathbf{A}_{10}(\boldsymbol{k}_t)$ and $\mathbf{B}_{nN+1}(\boldsymbol{k}_t) := \mathbf{B}_{nN}(\boldsymbol{k}_t) \cdot \mathbf{A}_{NN+1}(\boldsymbol{k}_t)$.

Equations (5.16) and (5.17) constitute the final set of equations for the case of several screen. The first equation, (5.16), is the most suitable for the analysis of the aperture case, while the second one, (5.17), is more adapted to the the patch case. These observations are exploited further below.

5.2 Special case — one screen ($N = 1$)

The case of one screen is special in that the screen has a half space on each side of it. There are, therefore, no interior screens, and we need to consider this case separately. Again, the goal of this section is to find the expression that relates the surface current on the screen, $\boldsymbol{J}_S(\boldsymbol{k}_t, z_1)$, to the electric field on the screen, $\boldsymbol{E}_{xy}(\boldsymbol{k}_t, z_1)$, and to the excitations of the entire slab, $\boldsymbol{F}^{+}(\boldsymbol{k}_t, z_0)$ and $\boldsymbol{F}^{-}(\boldsymbol{k}_t, z_2)$.

We let $N = 1$ and combine (5.12) and (5.13) to get

$$\begin{aligned} \eta_0 \boldsymbol{J}_S(\boldsymbol{k}_t, z_1) = &\mathbf{A}_{11}(\boldsymbol{k}_t) \cdot \boldsymbol{E}_{xy}(\boldsymbol{k}_t, z_1) \\ &+ \mathbf{A}_{10}(\boldsymbol{k}_t) \cdot \boldsymbol{F}^{+}(\boldsymbol{k}_t, z_0) + \mathbf{A}_{12}(\boldsymbol{k}_t) \cdot \boldsymbol{F}^{-}(\boldsymbol{k}_t, z_2) \end{aligned} \tag{5.18}$$

where

$$\begin{cases} \mathbf{A}_{11}(\boldsymbol{k}_t) = -\left((\mathbf{P}_{em} + \mathbf{W} \cdot \mathbf{P}_{mm})^{-1} \cdot (\mathbf{P}_{ee} + \mathbf{W} \cdot \mathbf{P}_{me})\right)(\boldsymbol{k}_t, z_2, z_1) \\ \qquad\qquad + \left((\mathbf{P}_{em} - \mathbf{W} \cdot \mathbf{P}_{mm})^{-1} \cdot (\mathbf{P}_{ee} - \mathbf{W} \cdot \mathbf{P}_{me})\right)(\boldsymbol{k}_t, z_0, z_1) \\ \mathbf{A}_{12}(\boldsymbol{k}_t) = 2(\mathbf{P}_{em} + \mathbf{W} \cdot \mathbf{P}_{mm})^{-1}(\boldsymbol{k}_t, z_2, z_1) \\ \boldsymbol{A}_{10}(\boldsymbol{k}_t) = -2(\mathbf{P}_{em} - \mathbf{W} \cdot \mathbf{P}_{mm})^{-1}(\boldsymbol{k}_t, z_0, z_1) \end{cases} \tag{5.19}$$

Equation (5.18) is a special case of (5.16) for one screen. It is, however, not possible to obtain this case from the general case.

The relation (5.18) can be inverted and the transverse electric field $\boldsymbol{E}_{xy}(\boldsymbol{k}_t, z_1)$ can be found in terms of the surface currents $\boldsymbol{J}_S(\boldsymbol{k}_t, z_1)$. The result is

$$\begin{aligned}\boldsymbol{E}_{xy}(\boldsymbol{k}_t, z_1) =& \mathbf{B}_{11}(\boldsymbol{k}_t) \cdot \eta_0 \boldsymbol{J}_S(\boldsymbol{k}_t, z_1) \\ &- \mathbf{B}_{10}(\boldsymbol{k}_t) \cdot \boldsymbol{F}^+(\boldsymbol{k}_t, z_0) - \mathbf{B}_{12}(\boldsymbol{k}_t) \cdot \boldsymbol{F}^-(\boldsymbol{k}_t, z_2)\end{aligned} \tag{5.20}$$

where

$$\begin{cases} \mathbf{B}_{11}(\boldsymbol{k}_t) = \mathbf{A}_{11}(\boldsymbol{k}_t)^{-1} \\ \mathbf{B}_{10}(\boldsymbol{k}_t) = \mathbf{B}_{11}(\boldsymbol{k}_t) \cdot \mathbf{A}_{10}(\boldsymbol{k}_t) \\ \mathbf{B}_{12}(\boldsymbol{k}_t) = \mathbf{B}_{11}(\boldsymbol{k}_t) \cdot \mathbf{A}_{12}(\boldsymbol{k}_t) \end{cases}$$

Equation (5.20) is a special case of (5.17) for the one screen case.

We can proceed further in the single screen case. Equation (5.20) can be combined with the the scattering equations (5.8) and (5.10) in order to eliminate the electric field $\boldsymbol{E}_{xy}(\boldsymbol{k}_t, z_1)$. The result is

$$\begin{cases} \boldsymbol{F}^-(\boldsymbol{k}_t, z_0) = \mathbf{r}_+(\boldsymbol{k}_t) \cdot \boldsymbol{F}^+(\boldsymbol{k}_t, z_0) + \mathbf{s}_+(\boldsymbol{k}_t) \cdot \eta_0 \boldsymbol{J}_S(\boldsymbol{k}_t, z_1) + \mathbf{t}_+(\boldsymbol{k}_t) \cdot \boldsymbol{F}^-(\boldsymbol{k}_t, z_2) \\ \boldsymbol{F}^+(\boldsymbol{k}_t, z_2) = \mathbf{t}_-(\boldsymbol{k}_t) \cdot \boldsymbol{F}^+(\boldsymbol{k}_t, z_0) + \mathbf{s}_-(\boldsymbol{k}_t) \cdot \eta_0 \boldsymbol{J}_S(\boldsymbol{k}_t, z_1) + \mathbf{r}_-(\boldsymbol{k}_t) \cdot \boldsymbol{F}^-(\boldsymbol{k}_t, z_2) \end{cases} \tag{5.21}$$

where

$$\begin{cases} \mathbf{r}_+(\boldsymbol{k}_t) = \mathbf{C}_0(\boldsymbol{k}_t) - \mathbf{C}_1(\boldsymbol{k}_t) \cdot \mathbf{A}_{11}(\boldsymbol{k}_t)^{-1} \cdot \mathbf{A}_{10}(\boldsymbol{k}_t) \\ \mathbf{s}_+(\boldsymbol{k}_t) = \mathbf{C}_1(\boldsymbol{k}_t) \cdot \mathbf{A}_{11}(\boldsymbol{k}_t)^{-1} \\ \mathbf{t}_+(\boldsymbol{k}_t) = -\mathbf{C}_1(\boldsymbol{k}_t) \cdot \mathbf{A}_{11}(\boldsymbol{k}_t)^{-1} \cdot \mathbf{A}_{12}(\boldsymbol{k}_t) \\ \mathbf{t}_-(\boldsymbol{k}_t) = -\mathbf{D}_1(\boldsymbol{k}_t) \cdot \mathbf{A}_{11}(\boldsymbol{k}_t)^{-1} \cdot \mathbf{A}_{10}(\boldsymbol{k}_t) \\ \mathbf{s}_-(\boldsymbol{k}_t) = \mathbf{D}_1(\boldsymbol{k}_t) \cdot \mathbf{A}_{11}(\boldsymbol{k}_t)^{-1} \\ \mathbf{r}_-(\boldsymbol{k}_t) = \mathbf{D}_2(\boldsymbol{k}_t) - \mathbf{D}_1(\boldsymbol{k}_t) \cdot \mathbf{A}_{11}(\boldsymbol{k}_t)^{-1} \cdot \mathbf{A}_{12}(\boldsymbol{k}_t) \end{cases} \tag{5.22}$$

In the absence of the screen, $\mathbf{r}_\pm(\boldsymbol{k}_t)$ and $\mathbf{t}_\pm(\boldsymbol{k}_t)$ are the reflection and transmission dyadics for the tangential electric field associated with plane-wave excitation of the bianisotropic slab [17].

5.2.1 Connection to reflection dyadics representation

The conventional way of solving scattering problems in planar geometries is by introducing the appropriate reflection and transmission dyadics of the slabs. As already should be obvious from above, this approach is not used in this paper. However, in this section we show how the reflection and the transmission dyadics can be identified from our approach for the one screen case. We like to stress that there are no advantages obtained in the numerical solution of the problem by such an identification, but there could be some pedagogical advantages in showing the connections to the more standard procedure. This identification parallels the connection in transmission line theory between the voltage-current or transmission (ABCD) matrix formulation and the scattering matrix formulation [3, 16].

Following [17] the reflection dyadic from the left, $\mathbf{r}$, and transmission dyadic for transmission from left to right, $\mathbf{t}$, for the tangential electric field are defined as

$$\begin{cases} \mathbf{r} = -\mathbf{T}_{mm}^{-1} \cdot \mathbf{T}_{me} \\ \mathbf{t} = \mathbf{T}_{ee} + \mathbf{T}_{em} \cdot \mathbf{r} \end{cases}$$

where

$$\begin{cases} 2\mathbf{T}_{ee} = \mathbf{P}_{ee} - \mathbf{P}_{em} \cdot \mathbf{W}^{-1} - \mathbf{W} \cdot \mathbf{P}_{me} + \mathbf{W} \cdot \mathbf{P}_{mm} \cdot \mathbf{W}^{-1} \\ 2\mathbf{T}_{em} = \mathbf{P}_{ee} + \mathbf{P}_{em} \cdot \mathbf{W}^{-1} - \mathbf{W} \cdot \mathbf{P}_{me} - \mathbf{W} \cdot \mathbf{P}_{mm} \cdot \mathbf{W}^{-1} \\ 2\mathbf{T}_{me} = \mathbf{P}_{ee} - \mathbf{P}_{em} \cdot \mathbf{W}^{-1} + \mathbf{W} \cdot \mathbf{P}_{me} - \mathbf{W} \cdot \mathbf{P}_{mm} \cdot \mathbf{W}^{-1} \\ 2\mathbf{T}_{mm} = \mathbf{P}_{ee} + \mathbf{P}_{em} \cdot \mathbf{W}^{-1} + \mathbf{W} \cdot \mathbf{P}_{me} + \mathbf{W} \cdot \mathbf{P}_{mm} \cdot \mathbf{W}^{-1} \end{cases}$$

and the propagators have the argument $(\boldsymbol{k}_t, z_2, z_1)$. In order to reproduce the result in [11], we let the excitation only come from the left, *i.e.*, $\boldsymbol{F}^-(\boldsymbol{k}_t, z_2) = \mathbf{0}$, and the support on the left hand side of the screen is vacuum, *i.e.*, the screen is supported only on the right hand side of the screen. Using equation (4.3) for the propagator $\mathbf{P}(\boldsymbol{k}_t, z_0, z_1)$, the expressions (5.19) and (5.9) reduce to

$$\begin{cases} \mathbf{A}_{11}(\boldsymbol{k}_t) = -\left((\mathbf{P}_{em} + \mathbf{W} \cdot \mathbf{P}_{mm})^{-1} \cdot (\mathbf{P}_{ee} + \mathbf{W} \cdot \mathbf{P}_{me})\right)(\boldsymbol{k}_t, z_2, z_1) - \mathbf{W}^{-1} \\ \boldsymbol{A}_{10}(\boldsymbol{k}_t) = 2\mathbf{W}^{-1} e^{-ik_z(z_0 - z_1)} \\ \mathbf{C}_0(\boldsymbol{k}_t) = -\mathbf{I}_2 e^{-2ik_z(z_0 - z_1)} \\ \mathbf{C}_1(\boldsymbol{k}_t) = \mathbf{I}_2 e^{-ik_z(z_0 - z_1)} \end{cases}$$

so that the dyadics in (5.22) become

$$\begin{cases} \mathbf{r}_+(\boldsymbol{k}_t) = -e^{-2ik_z(z_0 - z_1)} \left(\mathbf{I}_2 + 2\mathbf{A}_{11}(\boldsymbol{k}_t)^{-1} \cdot \mathbf{W}^{-1}\right) \\ \mathbf{s}_+(\boldsymbol{k}_t) = e^{-ik_z(z_0 - z_1)} \mathbf{A}_{11}(\boldsymbol{k}_t)^{-1} \end{cases}$$

However, it is straightforward to derive

$$\mathbf{A}_{11} = -2(\mathbf{P}_{em} + \mathbf{W} \cdot \mathbf{P}_{mm})^{-1} \cdot \mathbf{T}_{mm}$$

and

$$\mathbf{A}_{11}^{-1} = -\frac{1}{2}\mathbf{T}_{mm}^{-1} \cdot (\mathbf{T}_{mm} - \mathbf{T}_{me}) \cdot \mathbf{W} = -\frac{1}{2}(\mathbf{I}_2 + \mathbf{r}) \cdot \mathbf{W}$$

so that

$$\begin{cases} \mathbf{r}_+ = e^{-2ik_z(z_0 - z_1)} \mathbf{r} \\ \mathbf{s}_+ = -\frac{1}{2}(\mathbf{I}_2 + \mathbf{r}) \cdot \mathbf{W} e^{-ik_z(z_0 - z_1)} \end{cases}$$

The upper equation (5.21) then is

$$\boldsymbol{F}^-(z_0) = e^{-2ik_z(z_0 - z_1)} \mathbf{r} \cdot \boldsymbol{F}^+(z_0) - e^{-ik_z(z_0 - z_1)} \frac{1}{2}(\mathbf{I}_2 + \mathbf{r}) \cdot \mathbf{W} \cdot \eta_0 \boldsymbol{J}_S(z_1)$$

This expression is identical to the one in [11], since the exciting field $\boldsymbol{F}^+(z_0)$ in this case is identical to the incident field $\boldsymbol{E}_{xy}^i(z_0)$.

6 The Galerkin's method

In this section we show how the results from the previous sections can used to solve the aperture and patch cases. (The patch case is loosely defined as the cases when the minor part of each one of the scatterers is metallic, whereas we by the aperture case refer to the cases when the major part of each of the scatterers is metallic. When $N > 1$, this definition is, of course, not exhaustive.) We focus on the situation with a finite number of apertures or patches and employ the Galerkin's method. In Section 7 we address the case where the patches or apertures are periodically arranged, more explicitly, the frequency selective surface or structure case (FSS).

6.1 Aperture case

To solve the system (5.16), expand the transverse electric fields in the apertures in a complete set of expansion functions, *i.e.*,

$$\boldsymbol{E}_{xy}(\boldsymbol{\rho}, z_n) = \sum_l \alpha_l(z_n)\boldsymbol{e}_l(\boldsymbol{\rho}, z_n), \qquad n = 1, \cdots, N$$

where l typically is a two-dimensional multi-index. Note that this is an expansion of the transverse electric field in the physical domain, *i.e.*, the x-y-plane. The Fourier transform w.r.t. $\boldsymbol{\rho}$ of this expansion is

$$\boldsymbol{E}_{xy}(\boldsymbol{k}_t, z_n) = \sum_l \alpha_l(z_n)\boldsymbol{e}_l(\boldsymbol{k}_t, z_n), \qquad n = 1, \cdots, N$$

Let $\boldsymbol{w}_k(\boldsymbol{\rho}, z_n)$ be any vector-valued weight-function whose support is contained in the aperture of screen S_n. In the Galerkin's method we use

$$\boldsymbol{w}_k(\boldsymbol{\rho}, z_n) = \begin{cases} \boldsymbol{0} & \text{on the metallic parts of } S_n \\ \boldsymbol{e}_k(\boldsymbol{\rho}, z_n) & \text{in the apertures of } S_n \end{cases}$$

for $n = 1, \cdots, N$ and all multi-index k. Then

$$\iint_{-\infty}^{\infty} \boldsymbol{w}_k(\boldsymbol{\rho}, z_n)^* \cdot \boldsymbol{J}_S(\boldsymbol{\rho}, z_n)\, dx\, dy = 0, \qquad \text{for } n = 1, \cdots, N \text{ and all } k$$

Use the Parseval theorem

$$\int_{-\infty}^{\infty} f(x)^* g(x)\, dx = \frac{1}{2\pi} \int_{-\infty}^{\infty} f(k)^* g(k)\, dk$$

The result is

$$\iint_{-\infty}^{\infty} \boldsymbol{w}_k(\boldsymbol{k}_t, z_n)^* \cdot \boldsymbol{J}_S(\boldsymbol{k}_t, z_n)\, dk_x\, dk_y = 0, \qquad \text{for } n = 1, \cdots, N \text{ and all } k$$

in which equation (5.16) can be substituted and an infinite system of linear equations for the unknown $\alpha_l(z_m)$ is obtained:

$$\begin{aligned} 0 = &\sum_l \sum_{m=1}^{N} a_{nklm}\alpha_l(z_m) \\ &+ \delta_{n1} \iint_{-\infty}^{\infty} \boldsymbol{w}_k(\boldsymbol{k}_t, z_n)^* \cdot \mathbf{A}_{10}(\boldsymbol{k}_t) \cdot \boldsymbol{F}^+(\boldsymbol{k}_t, z_0)\, dk_x\, dk_y \\ &+ \delta_{nN} \iint_{-\infty}^{\infty} \boldsymbol{w}_k(\boldsymbol{k}_t, z_n)^* \cdot \mathbf{A}_{NN+1}(\boldsymbol{k}_t) \cdot \boldsymbol{F}^-(\boldsymbol{k}_t, z_{N+1})\, dk_x\, dk_y \end{aligned}$$

for $n = 1, \cdots, N$ and all multi-index k, where

$$a_{nklm} = \iint_{-\infty}^{\infty} \boldsymbol{w}_k(\boldsymbol{k}_t, z_n)^* \cdot \mathbf{A}_{nm}(\boldsymbol{k}_t) \cdot \boldsymbol{e}_l(\boldsymbol{k}_t, z_m)\, dk_x\, dk_y$$

6.2 Patch case

To proceed with the patch case (5.17), expand the currents fields at the screens in a complete set of expansion functions, *i.e.*,

$$\boldsymbol{J}_S(\boldsymbol{\rho}, z_k) = \sum_n \beta_n(z_k) \boldsymbol{j}_n(\boldsymbol{\rho}, z_k)$$

Note that this is an expansion of the surface current density in the physical domain, *i.e.*, the x-y-plane. The Fourier transform w.r.t. $\boldsymbol{\rho}$ is

$$\boldsymbol{J}_S(\boldsymbol{k}_t, z_k) = \sum_n \beta_n(z_k) \boldsymbol{j}_n(\boldsymbol{k}_t, z_k)$$

Let $\boldsymbol{w}_n(\boldsymbol{\rho}, z_k)$ be any vector-valued weight-function whose support is contained on the screens S_k. In the Galerkin's method we use

$$\boldsymbol{w}_n(\boldsymbol{\rho}, z_k) = \begin{cases} \mathbf{0} & \text{outside the metallic parts of } S_k \\ \boldsymbol{j}_n(\boldsymbol{\rho}, z_k) & \text{on the metallic parts of } S_k \end{cases}$$

Then

$$\iint_{-\infty}^{\infty} \boldsymbol{w}_n(\boldsymbol{\rho}, z_k)^* \cdot \boldsymbol{E}_{xy}(\boldsymbol{\rho}, z_k)\, dx\, dy = 0, \qquad k = 1, \cdots, N$$

Using the Parseval theorem gives the result

$$\iint_{-\infty}^{\infty} \boldsymbol{w}_n(\boldsymbol{k}_t, z_k)^* \cdot \boldsymbol{E}_{xy}(\boldsymbol{k}_t, z_k)\, dk_x\, dk_y = 0, \qquad k = 1, \cdots, N$$

in which equation (5.17) can be substituted and a system of equations for the unknown $\beta_n(z_k)$ is obtained.

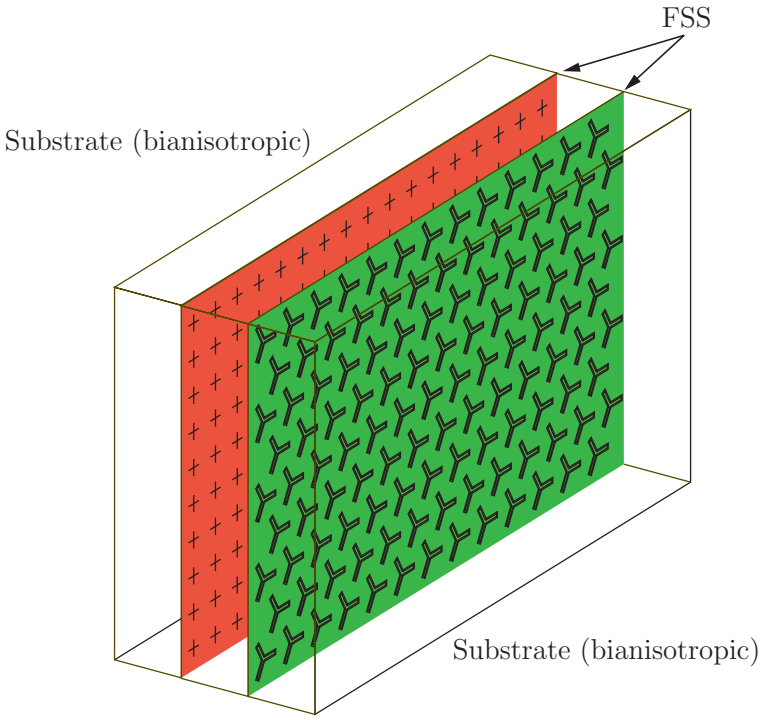

Figure 2: The geometry of a slab with two patch FSS supported by arbitrary, general slabs.

7 The periodic case — FSS

In the previous sections, we analyzed the case of a finite number of patches or apertures of arbitrary shape on each screen. We now let the number of patches or apertures on each screen be infinite, and, moreover, they are arranged in a periodic pattern on each screen. This situation comprises the important application of frequency selective surfaces or structures (FSS) [14].

To this end, we assume that all the patches or apertures on scatterer S_n are periodically distributed over the plane $z = z_n$ for $n = 1, 2, \ldots, N$, see also Figure 2. The periodicity is assumed to be the same or commensurate on all screens. Consequently, a unit cell relevant for all the screens can by defined by two linearly independent, lateral vectors, say $\boldsymbol{a} \in \mathbb{R}^2$ and $\boldsymbol{b} \in \mathbb{R}^2$ with lengths $a = |\boldsymbol{a}|$ and $b = |\boldsymbol{b}|$, respectively, see Figure 3. The periodic pattern can be obliquely oriented and ϕ_0 denotes the (smallest) angle between the axes of periodicity defined by $\cos\phi_0 = \boldsymbol{a} \cdot \boldsymbol{b}/(ab)$. We denote the unit cell by U, its area $A_U = |\boldsymbol{a} \times \boldsymbol{b}| = ab \sin\phi_0$, and the metallic parts in the unit cell by S_σ.

In the previous sections, the excitation was arbitrary and there could be sources on both sides of the slab, *i.e.*, in the regions $z < z_0$ and $z > z_{N+1}$. We now assume the incident wave to be a plane wave only from the left, *i.e.*, $\boldsymbol{F}^-(\boldsymbol{k}_t, z_{N+1}) = \boldsymbol{0}$.

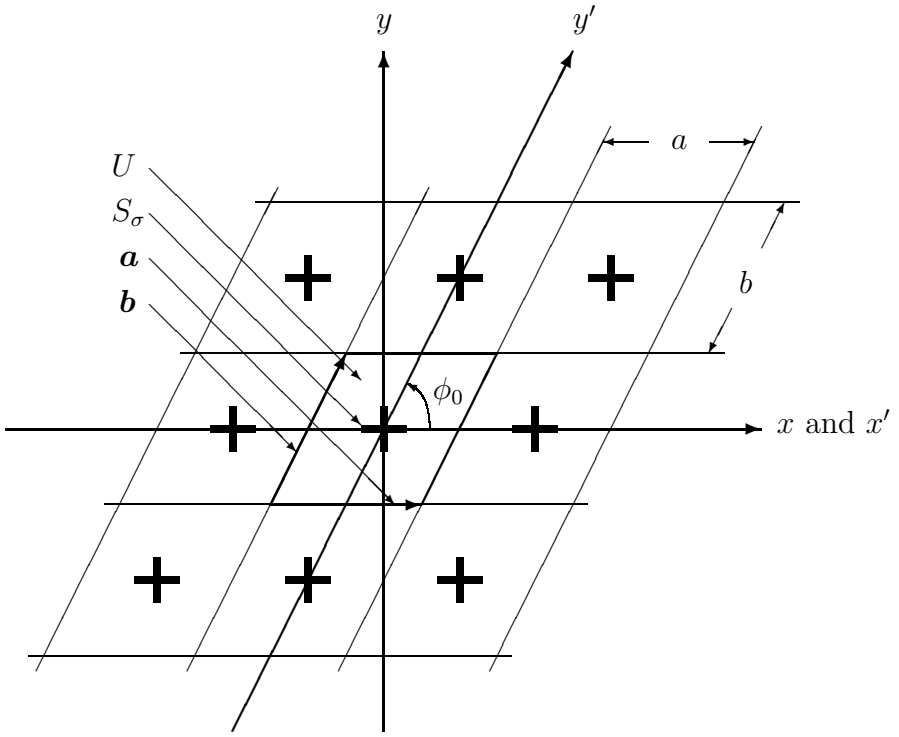

Figure 3: The unit cell U (patch case) generated by $\boldsymbol{a}$ and $\boldsymbol{b}$ with lengths $a = |\boldsymbol{a}|$ and $b = |\boldsymbol{b}|$.

Explicitly, we have

$$\boldsymbol{E}^i(\boldsymbol{r}) = \boldsymbol{E}^i_0 e^{i\boldsymbol{k}^i\cdot\boldsymbol{r}}$$

where $\boldsymbol{k}^i = k_0\hat{\boldsymbol{k}}^i$ is the constant real wave vector of the incident wave, and $\boldsymbol{E}^i_0$ is a constant complex vector, such that $\boldsymbol{E}^i_0 \cdot \boldsymbol{k}^i = 0$. The Fourier transform of the lateral part of this field evaluated at $z =$ constant is

$$\boldsymbol{F}^+(\boldsymbol{k}_t, z_0)e^{ik^i_z(z-z_0)} = \boldsymbol{E}^i_{xy}(\boldsymbol{k}_t, z) = 4\pi^2\boldsymbol{E}^i_{0xy}e^{ik^i_z z}\delta^2(\boldsymbol{k}_t - \boldsymbol{k}^i_t) \tag{7.1}$$

where the wave vector has been decomposed in lateral and longitudinal parts as $\boldsymbol{k}^i = \boldsymbol{k}^i_t + \hat{\boldsymbol{z}}k^i_z$, *i.e.*, $k^i_z = \boldsymbol{k}^i \cdot \hat{\boldsymbol{z}}$ and $\boldsymbol{k}^i_t = \mathbf{I}_2 \cdot \boldsymbol{k}^i$. The components of $\boldsymbol{k}^i$ in the x- and y-directions are denoted by k^i_x and k^i_y, respectively, *i.e.*, $\boldsymbol{k}^i_t = \hat{\boldsymbol{x}}k^i_x + \hat{\boldsymbol{y}}k^i_y$, and the spherical angles of $\boldsymbol{k}^i$ are denoted θ (polar angle) and ϕ (azimuth angle), *i.e.*, $\boldsymbol{k}^i = k_0(\hat{\boldsymbol{x}}\sin\theta\cos\phi + \hat{\boldsymbol{y}}\sin\theta\sin\phi + \hat{\boldsymbol{z}}\cos\theta)$.

To apply the results from the previous sections we need to find the relations between the Fourier transformed quantities used above and the Fourier coefficient of the pertinent periodic quantities that are appropriate in this section. To this end, Floquet's theorem [7] is applied. Consequently, the electric and magnetic fields and the current densities can be expanded in infinite exponential series with (lateral)

wave numbers ($\mathbb{Z}$ denotes the set of integers)

$$\boldsymbol{k}_{mn} = 2\pi \left(-m\frac{\hat{\boldsymbol{z}} \times \boldsymbol{b}}{\hat{\boldsymbol{z}} \cdot (\boldsymbol{a} \times \boldsymbol{b})} + n\frac{\hat{\boldsymbol{z}} \times \boldsymbol{a}}{\hat{\boldsymbol{z}} \cdot (\boldsymbol{a} \times \boldsymbol{b})} \right) + \boldsymbol{k}_t^i, \qquad m, n \in \mathbb{Z}$$

or if we adopt the notation of Appendix A

$$\boldsymbol{k}_{mn} = \boldsymbol{q}_{mn} + \boldsymbol{k}_t^i, \qquad m, n \in \mathbb{Z} \tag{7.2}$$

Notice that $\boldsymbol{k}_{00} = \boldsymbol{k}_t^i$. For the special geometry in Figure 3, where $\boldsymbol{a} = \hat{\boldsymbol{x}}a$ and $\boldsymbol{b} = \hat{\boldsymbol{x}}b\cos\phi_0 + \hat{\boldsymbol{y}}b\sin\phi_0$, we arrive the result presented in [15], namely $\boldsymbol{k}_{mn} = \hat{\boldsymbol{x}}\alpha_m + \hat{\boldsymbol{y}}\beta_{mn}$ with

$$\begin{cases} \alpha_m = \dfrac{2\pi m}{a} + k_x^i \\ \beta_{mn} = \dfrac{2\pi n}{b\sin\phi_0} - \dfrac{2\pi m}{a}\cot\phi_0 + k_y^i \end{cases} \qquad m, n \in \mathbb{Z}$$

Applying Floquet's theorem [7] to the induced surface current densities at the screens, $\boldsymbol{J}_S(\boldsymbol{\rho}, z_j) = \mathbf{J} \cdot \big(\boldsymbol{H}(\boldsymbol{\rho}, z_j^+) - \boldsymbol{H}(\boldsymbol{\rho}, z_j^-)\big)$, which in non-zero on the metallic parts, S_σ, and zero elsewhere on the plane $z = z_j$, gives

$$\boldsymbol{J}_S(\boldsymbol{\rho}, z_j) = \frac{1}{A_U} \sum_{m,n=-\infty}^{\infty} \boldsymbol{J}_S|_U(\boldsymbol{k}_{mn}, z_j) e^{i\boldsymbol{k}_{mn}\cdot\boldsymbol{\rho}}, \qquad j = 1, 2, \ldots, N, \quad \boldsymbol{\rho} \in \mathbb{R}^2$$

where the lateral wave numbers $\boldsymbol{k}_{mn}$ are given by equation (7.2), and the coefficient $\boldsymbol{J}_S|_U(\boldsymbol{k}_{mn}, z_j)$ is the lateral Fourier transform of $\boldsymbol{J}_S(\boldsymbol{\rho}, z_j)$ restricted to the unit cell U and evaluated at $\boldsymbol{k}_{mn}$, *i.e.*,

$$\boldsymbol{J}_S|_U(\boldsymbol{k}_{mn}, z_j) = \iint_U \boldsymbol{J}_S(\boldsymbol{\rho}, z_j) e^{-i\boldsymbol{k}_{mn}\cdot\boldsymbol{\rho}} dxdy, \qquad j = 1, 2, \ldots, N$$

Notice that this quantity is identical to the Fourier coefficient, (A.1), of the periodic function $\boldsymbol{J}_S(\boldsymbol{\rho}, z_j)e^{-i\boldsymbol{k}_t^i\cdot\boldsymbol{\rho}}$. The symbol $|_U$ is used here and below to emphasize that the quantity is a lateral Fourier transform of an aperiodic quantity with support in the unit cell U and to distinguish between $\boldsymbol{J}_S(\boldsymbol{k}_t, z_j)$ and $\boldsymbol{J}_S|_U(\boldsymbol{k}_{mn}, z_j)$. Consequently, the connection between the lateral Fourier transforms of the surface current densities, $\boldsymbol{J}_S(\boldsymbol{k}_t, z_j)$, and its restriction to the unit cell, $\boldsymbol{J}_S|_U(\boldsymbol{k}_{mn}, z_j)$, is, *cf.* (3.1)

$$\boldsymbol{J}_S(\boldsymbol{k}_t, z_j) = \frac{4\pi^2}{A_U} \sum_{m,n=-\infty}^{\infty} \boldsymbol{J}_S|_U(\boldsymbol{k}_{mn}, z_j)\delta^2(\boldsymbol{k}_t - \boldsymbol{k}_{mn}), \qquad j = 1, 2, \ldots, N \tag{7.3}$$

This connection can now be used in the results in the previous sections.

Similarly, applying Floquet's theorem to the lateral electric fields at the screens, $\boldsymbol{E}_{xy}(\boldsymbol{\rho}, z_j)$, yields

$$\boldsymbol{E}_{xy}(\boldsymbol{\rho}, z_j) = \frac{1}{A_U} \sum_{m,n=-\infty}^{\infty} \boldsymbol{E}_{xy}|_U(\boldsymbol{k}_{mn}, z_j) e^{i\boldsymbol{k}_{mn}\cdot\boldsymbol{\rho}}, \qquad j = 1, 2, \ldots, N$$

where the coefficients $\boldsymbol{E}_{xy}|_U(\boldsymbol{k}_{mn}, z_j)$ are the lateral Fourier transform of $\boldsymbol{E}_{xy}(\boldsymbol{\rho}, z_j)$ restricted to the unit cell U and evaluated at $\boldsymbol{k}_{mn}$, *i.e.*,

$$\boldsymbol{E}_{xy}|_U(\boldsymbol{k}_{mn}, z_j) = \iint_U \boldsymbol{E}_{xy}(\boldsymbol{\rho}, z_j) e^{-i\boldsymbol{k}_{mn}\cdot\boldsymbol{\rho}} dxdy, \qquad j = 1, 2, \ldots, N$$

Consequently, the lateral Fourier transforms of the lateral electric fields are

$$\boldsymbol{E}_{xy}(\boldsymbol{k}_t, z_j) = \frac{4\pi^2}{A_U} \sum_{m,n=-\infty}^{\infty} \boldsymbol{E}_{xy}|_U(\boldsymbol{k}_{mn}, z_j)\delta^2(\boldsymbol{k}_t - \boldsymbol{k}_{mn}), \qquad j = 1, 2, \ldots, N \quad (7.4)$$

Finally, since $\boldsymbol{k}_t^i = \boldsymbol{k}_{00}$, the excitation from the left (7.1) can be written as

$$\boldsymbol{F}^+(\boldsymbol{k}_t, z_0) = 4\pi^2 \boldsymbol{F}^+(\boldsymbol{k}_{00}, z_0)\delta^2(\boldsymbol{k}_t - \boldsymbol{k}_{00}) \quad (7.5)$$

where $\boldsymbol{F}^+(\boldsymbol{k}_{00}, z_0) = \boldsymbol{E}_{0xy}^i e^{ik_z^i z_0}$.

7.1 Patch case

We begin the analysis of the FSS with the patch case. Substituting equations (7.3), (7.4), and (7.5) into the relation (5.17) between the electric fields, the surface current densities, and the excitation from the left gives

$$\begin{aligned} \boldsymbol{E}_{xy}|_U(\boldsymbol{k}_{mn}, z_j) = &\sum_{k=1}^{N} \mathbf{B}_{jk}(\boldsymbol{k}_{mn}) \cdot \eta_0 \boldsymbol{J}_S|_U(\boldsymbol{k}_{mn}, z_k) \\ &- A_U \mathbf{B}_{j0}(\boldsymbol{k}_{00}) \cdot \boldsymbol{F}^+(\boldsymbol{k}_{00}, z_0)\delta_{m0}\delta_{n0}, \qquad j = 1, 2, \ldots, N \end{aligned} \quad (7.6)$$

where the $\mathbf{B}$-matrices were defined in Section 5.1. This equation holds when $N > 1$. When $N = 1$, plugging into (5.20) gives an identical result

$$\boldsymbol{E}_{xy}|_U(\boldsymbol{k}_{mn}, z_1) = \mathbf{B}_{11}(\boldsymbol{k}_{mn}) \cdot \eta_0 \boldsymbol{J}_S|_U(\boldsymbol{k}_{mn}, z_1) - A_U \mathbf{B}_{10}(\boldsymbol{k}_{00}) \cdot \boldsymbol{F}^+(\boldsymbol{k}_{00}, z_0)\delta_{m0}\delta_{n0}$$

where the $\mathbf{B}$-matrices were defined in Section 5.2.

The current density $\boldsymbol{J}_S(\boldsymbol{\rho}, z_j)$ can be expanded with arbitrary precision in a pertinent complete set of entire domain or local basis functions $\boldsymbol{j}_p(\boldsymbol{\rho}, z_j)$ (supported on the patches), *i.e.*,

$$\boldsymbol{J}_S(\boldsymbol{\rho}, z_j) = \sum_{p\in\chi} C_p^j \boldsymbol{j}_p(\boldsymbol{\rho}, z_j), \qquad j = 1, 2, \ldots, N;\ \boldsymbol{\rho} \in U$$

where χ is a set of indices (countable set) and the scalars C_p^j are the unknown expansion coefficients. It suffices to define the basis functions $\boldsymbol{j}_p(\boldsymbol{\rho}, z_j)$ in the unit cell U. The lateral Fourier transform of this expansion is

$$\boldsymbol{J}_S|_U(\boldsymbol{k}_{mn}, z_j) = \sum_{p\in\chi} C_p^j \boldsymbol{j}_p(\boldsymbol{k}_{mn}, z_j), \qquad j = 1, 2, \ldots, N$$

where

$$\boldsymbol{j}_p(\boldsymbol{k}_{mn}, z_j) = \iint\limits_U \boldsymbol{j}_p(\boldsymbol{\rho}, z_j) e^{-i\boldsymbol{k}_{mn}\cdot\boldsymbol{\rho}} dxdy, \qquad j = 1, 2, \ldots, N;\ p \in \chi$$

We assume that an appropriate set of weight functions $\boldsymbol{w}_p(\boldsymbol{\rho}, z_j)$ (supported on the patches) has been defined. In the Galerkin's method the functions $\boldsymbol{j}_p(\boldsymbol{\rho}, z_j)$ are used. The lateral Fourier transform of the weight functions $\boldsymbol{w}_p(\boldsymbol{\rho}, z_j)$ is defined as

$$\boldsymbol{w}_p(\boldsymbol{k}_{mn}, z_j) = \iint\limits_U \boldsymbol{w}_p(\boldsymbol{\rho}, z_j) e^{-i\boldsymbol{k}_{mn}\cdot\boldsymbol{\rho}} dxdy, \qquad j = 1, 2, \ldots, N$$

In complete analogy with the result in Section 6, we have

$$\iint\limits_U \boldsymbol{w}_p(\boldsymbol{\rho}, z_j)^* \cdot \boldsymbol{E}_{xy}(\boldsymbol{\rho}, z_j)\, dx\, dy = 0, \qquad j = 1, 2, \ldots, N;\ p \in \chi$$

and modifying the Parseval theorem (A.2) for Fourier series to Floquet expansions gives

$$\sum_{m,n=-\infty}^{\infty} \boldsymbol{w}_p(\boldsymbol{k}_{mn}, z_j)^* \cdot \boldsymbol{E}_{xy}|_U(\boldsymbol{k}_{mn}, z_j) = 0, \qquad j = 1, 2, \ldots, N;\ p \in \chi$$

in which equation (7.6) can be substituted and a system of equations for the unknown C_p^j is obtained. Specifically,

$$\begin{aligned}\sum_{m,n=-\infty}^{\infty} \boldsymbol{w}_p(\boldsymbol{k}_{mn}, z_j)^* \cdot \sum_{k=1}^{N} \mathbf{B}_{jk}(\boldsymbol{k}_{mn}) \cdot \eta_0 \sum_{q\in\chi} C_q^k \boldsymbol{j}_q(\boldsymbol{k}_{mn}, z_k)& \\ = A_U \boldsymbol{w}_p(\boldsymbol{k}_{00}, z_j)^* \cdot \mathbf{B}_{j0}(\boldsymbol{k}_{00}) \cdot \boldsymbol{F}^+(\boldsymbol{k}_{00}, z_0), \qquad j = 1, 2, \ldots, N;\ p \in \chi&\end{aligned}$$

If χ is an infinite set of indices, the above equation is an infinite system of linear equations for the unknown current coefficients C_q^k. We assume that if this infinite system is truncated, the solution to the truncated system approximates the exact solution. An excellent treatment of the convergence properties of the Galerkin's method (and other projection methods) is found in [10]. When the linear system is truncated, it can be written as

$$\mathbf{A}\boldsymbol{C} = \boldsymbol{b}$$

where $\mathbf{A}$ is a square matrix, $\boldsymbol{C}$ is a vector containing the unknown coefficients C_q^k, and $\boldsymbol{b}$ is a known vector. Specifically, the matrix elements are

$$\begin{aligned}A_{jp,kq} = \eta_0 \sum_{m,n=-\infty}^{\infty} \boldsymbol{w}_p(\boldsymbol{k}_{mn}, z_j)^* \cdot \mathbf{B}_{jk}(\boldsymbol{k}_{mn}) \cdot \boldsymbol{j}_q(\boldsymbol{k}_{mn}, z_k)& \\ j, k = 1, 2, \ldots, N;\ p, q \in \chi&\end{aligned}$$

and the right-hand entries are

$$b_{jp} = A_U \boldsymbol{w}_p(\boldsymbol{k}_{00}, z_j)^* \cdot \mathbf{B}_{j0}(\boldsymbol{k}_{00}) \cdot \boldsymbol{F}^+(\boldsymbol{k}_{00}, z_0), \qquad j = 1, 2, \ldots, N;\ p \in \chi$$

7.2 Aperture case

The aperture case follows a similar analysis as the patch case in Section 7.1. Substituting equations (7.3), (7.4), and (7.5) into the relation (5.16) between the electric fields, the surface current densities, and the excitation from the left gives

$$\begin{aligned}\eta_0 \boldsymbol{J}_S|_U(\boldsymbol{k}_{mn}, z_j) = &\sum_{k=1}^{N} \mathbf{A}_{jk}(\boldsymbol{k}_{mn}) \cdot \boldsymbol{E}_{xy}|_U(\boldsymbol{k}_{mn}, z_k) \\ &+ A_U \mathbf{A}_{10}(\boldsymbol{k}_{00}) \cdot \boldsymbol{F}^+(\boldsymbol{k}_{00}, z_0)\delta_{m0}\delta_{n0}\delta_{j1}, \qquad j = 1, 2, \ldots, N\end{aligned} \tag{7.7}$$

where the **A**-matrices were defined by (5.5) and in Section 5.1. This equation holds when $N > 1$. When $N = 1$, (5.18) gives a similar result

$$\eta_0 \boldsymbol{J}_S|_U(\boldsymbol{k}_{mn}, z_1) = \mathbf{A}_{11}(\boldsymbol{k}_{mn}) \cdot \boldsymbol{E}_{xy}|_U(\boldsymbol{k}_{mn}, z_1) + A_U \mathbf{A}_{10}(\boldsymbol{k}_{00}) \cdot \boldsymbol{F}^+(\boldsymbol{k}_{00}, z_0)\delta_{m0}\delta_{n0}$$

where the **A**-matrices were defined in Section 5.2.

In analogy with the patch case, the electric field $\boldsymbol{E}_{xy}(\boldsymbol{\rho}, z_j)$ can be expanded with arbitrary precision in a pertinent complete set of entire domain or local basis functions $\boldsymbol{e}_p(\boldsymbol{\rho}, z_j)$ (supported on the apertures), *i.e.*,

$$\boldsymbol{E}_{xy}(\boldsymbol{\rho}, z_j) = \sum_{p \in \chi} D_p^j \boldsymbol{e}_p(\boldsymbol{\rho}, z_j), \qquad j = 1, 2, \ldots, N;\ \boldsymbol{\rho} \in E$$

where χ is a set of indices (countable set) and the scalars D_p^j are the unknown expansion coefficients. It suffices to define the basis functions $\boldsymbol{e}_p(\boldsymbol{\rho}, z_j)$ in the unit cell U. The lateral Fourier transform of this expansion is

$$\boldsymbol{E}_{xy}|_U(\boldsymbol{k}_{mn}, z_j) = \sum_{p \in \chi} D_p^j \boldsymbol{e}_p(\boldsymbol{k}_{mn}, z_j), \qquad j = 1, 2, \ldots, N;\ p \in \chi$$

where

$$\boldsymbol{e}_p(\boldsymbol{k}_{mn}, z_j) = \iint_U \boldsymbol{e}_p(\boldsymbol{\rho}, z_j) e^{-i\boldsymbol{k}_{mn}\cdot\boldsymbol{\rho}} dxdy, \qquad j = 1, 2, \ldots, N;\ p \in \chi$$

We assume that appropriate weight functions $\boldsymbol{w}_p(\boldsymbol{\rho}, z_j)$ (supported on the apertures) are defined. In the Galerkin's method the functions $\boldsymbol{e}_p(\boldsymbol{\rho}, z_j)$ are used. The lateral Fourier transform of the weight functions $\boldsymbol{w}_p(\boldsymbol{\rho}, z_j)$ is defined as

$$\boldsymbol{w}_p(\boldsymbol{k}_{mn}, z_j) = \iint_U \boldsymbol{w}_p(\boldsymbol{\rho}, z_j) e^{-i\boldsymbol{k}_{mn}\cdot\boldsymbol{\rho}} dxdy, \qquad j = 1, 2, \ldots, N$$

In complete analogy to above, we have

$$\iint_U \boldsymbol{w}_p(\boldsymbol{\rho}, z_j)^* \cdot \boldsymbol{J}_S(\boldsymbol{\rho}, z_j)\, dx\, dy = 0, \qquad j = 1, 2, \ldots, N;\ p \in \chi$$

and consequently

$$\sum_{m,n=-\infty}^{\infty} \boldsymbol{w}_p(\boldsymbol{k}_{mn}, z_j)^* \cdot \boldsymbol{J}_S|_U(\boldsymbol{k}_{mn}, z_j) = 0, \qquad j = 1, 2, \ldots, N;\ p \in \chi$$

in which equation (7.7) can be substituted and a system of equations for the unknown D_q^k is obtained. Specifically,

$$\begin{aligned}\sum_{m,n=-\infty}^{\infty} \boldsymbol{w}_p(\boldsymbol{k}_{mn}, z_j)^* \cdot \sum_{k=1}^{N} \mathbf{A}_{jk}(\boldsymbol{k}_{mn}) \cdot \sum_{q\in\chi} D_q^k \boldsymbol{e}_q(\boldsymbol{\rho}, z_k) \\ = -A_U \boldsymbol{w}_p(\boldsymbol{k}_{00}, z_j)^* \cdot \mathbf{A}_{10}(\boldsymbol{k}_{00}) \cdot \boldsymbol{F}^+(\boldsymbol{k}_{00}, z_0)\delta_{j1}, \qquad j = 1, 2, \ldots, N;\ p \in \chi\end{aligned}$$

This system of linear equations can be written as

$$\mathbf{A}\boldsymbol{D} = \boldsymbol{b}$$

where $\mathbf{A}$ is a square matrix, $\boldsymbol{D}$ is a vector containing the unknown coefficients D_q^k, and $\boldsymbol{b}$ is a known vector. Specifically, the matrix elements are

$$\begin{aligned}A_{jp,kq} = \sum_{m,n=-\infty}^{\infty} \boldsymbol{w}_p(\boldsymbol{k}_{mn}, z_j)^* \cdot \mathbf{A}_{jk}(\boldsymbol{k}_{mn}) \cdot \boldsymbol{e}_q(\boldsymbol{\rho}, z_k) \\ j, k = 1, 2, \ldots, N;\ p, q \in \chi\end{aligned}$$

and the right-hand entries are

$$b_{jp} = -A_U \boldsymbol{w}_p(\boldsymbol{k}_{00}, z_j)^* \cdot \mathbf{A}_{10}(\boldsymbol{k}_{00}) \cdot \boldsymbol{F}^+(\boldsymbol{k}_{00}, z_0)\delta_{j1}, \qquad j = 1, 2, \ldots, N;\ p \in \chi$$

7.3 The reflection and transmission coefficients

In this section we derive an explicit expression of the field in each of the two half spaces, $z < z_0$, and, $z > z_{N+1}$, respectively, in terms of the transverse electric field on $z = z_1$ and $z = z_N$.

The Galerkin method presented in Sections 7.1 and 7.2 provides us with an approximation of the transverse electric field at $z = z_1$ and $z = z_N$. In the aperture case this is the direct output of the numerical calculations. In the patch case we have an expression of the surface currents on the metal patches. However, this quantity is easily transformed into the transverse electric field by (5.17). Therefore, the fields $\boldsymbol{E}_{xy}(\boldsymbol{\rho}, z_j)$, $j = 1, 2, \ldots, N$, are known, or even more appropriate, their Fourier transform $\boldsymbol{E}_{xy}(\boldsymbol{k}_{mn}, z_j)$. The relation to the Fourier transform of the fields $\boldsymbol{E}_{xy}(\boldsymbol{k}_t, z_j)$ is, see (7.4)

$$\boldsymbol{E}_{xy}(\boldsymbol{k}_t, z_j) = \frac{4\pi^2}{A_U} \sum_{m,n=-\infty}^{\infty} \boldsymbol{E}_{xy}|_U(\boldsymbol{k}_{mn}, z_j)\delta^2(\boldsymbol{k}_t - \boldsymbol{k}_{mn}), \quad j = 1, 2, \ldots, N$$

The relation between the scattered field $\boldsymbol{F}^-(\boldsymbol{k}_t, z)$ in the half space $z < z_0$ and the electric field on the $z = z_1$ is given by (5.8), and the relation between the scattered field $\boldsymbol{F}^+(\boldsymbol{k}_t, z)$ in the half space $z > z_{N+1}$ and the electric field on the $z = z_N$ is given by (5.10), *i.e.*,

$$\begin{cases} \boldsymbol{F}^-(\boldsymbol{k}_t, z) = \big(\mathbf{C}_0(\boldsymbol{k}_t) \cdot \boldsymbol{F}^+(\boldsymbol{k}_t, z_0) + \mathbf{C}_1(\boldsymbol{k}_t) \cdot \boldsymbol{E}_{xy}(\boldsymbol{k}_t, z_1)\big)\, e^{-ik_z(z-z_0)} \\ \boldsymbol{F}^+(\boldsymbol{k}_t, z) = \big(\mathbf{D}_{N+1}(\boldsymbol{k}_t) \cdot \boldsymbol{F}^-(\boldsymbol{k}_t, z_{N+1}) + \mathbf{D}_N(\boldsymbol{k}_t) \cdot \boldsymbol{E}_{xy}(\boldsymbol{k}_t, z_N)\big)\, e^{ik_z(z-z_{N+1})} \end{cases}$$

where the explicit expressions of the dyadics $\mathbf{C}_0$, $\mathbf{C}_1$, $\mathbf{D}_{N-1}$, and $\mathbf{D}_N$, are given in Section 5.

As above, we restrict ourselves to an incident field from the left, $\boldsymbol{F}^-(\boldsymbol{k}_t, z_{N+1}) = \mathbf{0}$, see (7.1). From the split fields in the half spaces we identify the reflected and the transmitted fields, $\boldsymbol{E}^r(\boldsymbol{k}_t, z)$ and $\boldsymbol{E}^t(\boldsymbol{k}_t, z)$, respectively, by the projection operator[7]

$$\boldsymbol{\gamma}^{\pm}(\boldsymbol{k}_t) = \mathbf{I}_2 \mp \hat{\boldsymbol{z}} \frac{1}{k_0} \boldsymbol{k}_t \cdot \mathbf{W}^{-1} \tag{7.8}$$

which is used to reconstruct the z-component from the tangential field. We have

$$\begin{cases} \boldsymbol{E}^r(\boldsymbol{k}_t, z) = \boldsymbol{\gamma}^-(\boldsymbol{k}_t) \cdot \big(\mathbf{C}_0(\boldsymbol{k}_t) \cdot \boldsymbol{F}^+(\boldsymbol{k}_t, z_0) + \mathbf{C}_1(\boldsymbol{k}_t) \cdot \boldsymbol{E}_{xy}(\boldsymbol{k}_t, z_1)\big)\, e^{-ik_z(z-z_0)} \\ \boldsymbol{E}^t(\boldsymbol{k}_t, z) = \boldsymbol{\gamma}^+(\boldsymbol{k}_t) \cdot \mathbf{D}_N(\boldsymbol{k}_t) \cdot \boldsymbol{E}_{xy}(\boldsymbol{k}_t, z_N) e^{ik_z(z-z_{N+1})} \end{cases}$$

The field at a point $\boldsymbol{r}$ such that $z < z_0$ is given by[8]

$$\boldsymbol{E}^r(\boldsymbol{r}) = \frac{1}{4\pi^2} \iint_{-\infty}^{\infty} \boldsymbol{E}^r(\boldsymbol{k}_t, z_0) e^{i\boldsymbol{k}_t \cdot \boldsymbol{\rho} - ik_z(z-z_0)}\, dk_x\, dk_y$$

and for a point $z > z_{N+1}$ the field is given by

$$\boldsymbol{E}^t(\boldsymbol{r}) = \frac{1}{4\pi^2} \iint_{-\infty}^{\infty} \boldsymbol{E}^t(\boldsymbol{k}_t, z_{N+1}) e^{i\boldsymbol{k}_t \cdot \boldsymbol{\rho} + ik_z(z-z_{N+1})}\, dk_x\, dk_y$$

We introduce the wave vector of the transmitted and reflected field as

$$\boldsymbol{k}_{mn}^{\pm} = \boldsymbol{k}_{mn} \pm \hat{\boldsymbol{z}} k_{zmn}, \qquad m, n \in \mathbb{Z}$$

where

$$k_{zmn} = \big(k_0^2 - |\boldsymbol{k}_{mn}|^2\big)^{1/2} = \begin{cases} \sqrt{k_0^2 - |\boldsymbol{k}_{mn}|^2} \text{ for } |\boldsymbol{k}_{mn}| < k_0 \\ i\sqrt{|\boldsymbol{k}_{mn}|^2 - k_0^2} \text{ for } |\boldsymbol{k}_{mn}| > k_0 \end{cases}$$

[7]The total electric field in a vacuous region is

$$\boldsymbol{E}(\boldsymbol{k}_t, z) = \boldsymbol{E}_{xy}(\boldsymbol{k}_t, z) + \hat{\boldsymbol{z}} \frac{\eta_0}{k_0} \boldsymbol{k}_t \cdot \mathbf{J} \cdot \boldsymbol{H}_{xy}(\boldsymbol{k}_t, z) = \boldsymbol{E}_{xy}(\boldsymbol{k}_t, z) \mp \hat{\boldsymbol{z}} \frac{1}{k_0} \boldsymbol{k}_t \cdot \mathbf{W}^{-1} \cdot \boldsymbol{E}_{xy}(\boldsymbol{k}_t, z)$$

[8]Any poles along the integration contour, which reflects the presence of a surface mode, must be avoided by an appropriate deformation of the contour, see [6, 12].

Note that $k_z^i = k_{z00}$. Then, from (7.4) and (7.5) we obtain

$$\boldsymbol{E}^r(\boldsymbol{r}) = \left(\mathbf{S}^- \cdot \boldsymbol{E}^i_{0xy}\right) e^{i\boldsymbol{k}^-_{00}\cdot\boldsymbol{r}} + \sum_{m,n=-\infty}^{\infty} \mathbf{G}^-_{mn} \cdot \boldsymbol{E}_{xy}|_U(\boldsymbol{k}_{mn}, z_1) e^{i\boldsymbol{k}^-_{mn}\cdot\boldsymbol{r}}, \quad z < z_0$$

where

$$\begin{cases} \mathbf{S}^- = \boldsymbol{\gamma}^-(\boldsymbol{k}_{00}) \cdot \mathbf{C}_0(\boldsymbol{k}_{00}) e^{2ik_{z00}z_0} \\ \mathbf{G}^-_{mn} = \dfrac{1}{A_U} \boldsymbol{\gamma}^-(\boldsymbol{k}_{mn}) \cdot \mathbf{C}_1(\boldsymbol{k}_{mn}) e^{ik_{zmn}z_0} \end{cases}$$

where we also used $\boldsymbol{F}^+(\boldsymbol{k}_{00}, z_0) = \boldsymbol{E}^i_{0xy} e^{ik^i_z z_0} = \boldsymbol{E}^i_{0xy} e^{ik_{z00}z_0}$.

In order to identify the reflection dyadic of the FSS and the substrate, we introduce the dyadic $\mathbf{C}^-_{mn}$ implicitly defined by

$$\mathbf{C}^-_{mn} \cdot \boldsymbol{E}^i_{0xy} = \mathbf{G}^-_{mn} \cdot \boldsymbol{E}_{xy}|_U(\boldsymbol{k}_{mn})$$

This definition enables us to define the reflection dyadic $\mathbf{R}_{mn}$ of the FSS and the slab as

$$\mathbf{R}_{mn} = \mathbf{S}^- \delta_{m0}\delta_{n0} + \mathbf{C}^-_{mn}$$

The co- and cross-polarized components of the reflection dyadic are

$$\hat{\boldsymbol{e}}_i(\boldsymbol{k}_{mn}) \cdot \mathbf{R}_{mn} \cdot \hat{\boldsymbol{e}}_j(\boldsymbol{k}_{mn})$$

The $i = \parallel$ $(i = \perp)$ and $j = \parallel$ $(j = \perp)$ are the co-polarized TM (TE) contributions. The off diagonal parts give the cross-polarizations. The fundamental mode corresponds to $m = n = 0$.

Only the propagating part of the field ($|\boldsymbol{k}_{mn}| < k_0$) contributes to the far field. If $|\boldsymbol{k}_{mn}| > k_0$ for all $(m, n) \neq (0, 0)$, we have no grating lobes. This is the case of most technical interest. Assuming this is the case, we have the reflectance R of the FSS defined as

$$\begin{aligned} R &= \lim_{z\to-\infty} \frac{\left|\boldsymbol{E}^r(\boldsymbol{r})\right|^2}{\left|\boldsymbol{E}^i_0\right|^2} \\ &= \frac{\left|\mathbf{S}^- \cdot \boldsymbol{E}^i_{0xy} + \mathbf{G}^-_{00} \cdot \boldsymbol{E}_{xy}|_U(\boldsymbol{k}_{00})\right|^2}{\left|\boldsymbol{E}^i_0\right|^2} = \frac{\left|\mathbf{R}_{00} \cdot \boldsymbol{E}^i_{0xy}\right|^2}{\left|\boldsymbol{E}^i_0\right|^2}, \qquad \text{no grating lobes} \end{aligned}$$

We now proceed and calculate the transmitted field and use (7.3).

$$\boldsymbol{E}^t(\boldsymbol{r}) = \sum_{m,n=-\infty}^{\infty} \mathbf{G}^+_{mn} \cdot \boldsymbol{E}_{xy}|_U(\boldsymbol{k}_{mn}, z_N) e^{\boldsymbol{k}^+_{mn}\cdot\boldsymbol{r}}, \quad z > z_{N+1}$$

where

$$\mathbf{G}^+_{mn} = \frac{1}{A_U} \boldsymbol{\gamma}^+(\boldsymbol{k}_{mn}) \cdot \mathbf{D}_N(\boldsymbol{k}_{mn}) e^{-ik_{zmn}z_{N+1}}$$

Analogous to the reflection dyadic defined above, we introduce the transmission dyadic of the FSS and the substrate. To this end, the dyadic $\mathbf{C}^+_{mn}$ is implicitly defined by

$$\mathbf{C}^+_{mn} \cdot \boldsymbol{E}^i_{0xy} = \mathbf{G}^+_{mn} \cdot \boldsymbol{E}_{xy}|_U(\boldsymbol{k}_{mn}, z_N)$$

This definition enables us to define the transmission dyadic $\mathbf{T}_{mn}$ of the FSS and the slab as

$$\mathbf{T}_{mn} = \mathbf{C}^+_{mn}$$

The co- and cross-polarized components of the transmission dyadic are

$$\hat{\boldsymbol{e}}_i(\boldsymbol{k}_{mn}) \cdot \mathbf{T}_{mn} \cdot \hat{\boldsymbol{e}}_j(\boldsymbol{k}_{mn})$$

The $i = \parallel$ ($i = \perp$) and $j = \parallel$ ($j = \perp$) are the co-polarized TM (TE) contributions. The off diagonal parts give the cross-polarizations. The fundamental mode corresponds to $m = n = 0$.

As before, only the propagating part of the field ($|\boldsymbol{k}_{mn}| < k_0$) contributes to the far field. In the absence of grating lobes, we have the transmittance T of the FSS defined as

$$\begin{aligned} T &= \lim_{z\to\infty} \frac{\left|\boldsymbol{E}^t(\boldsymbol{r})\right|^2}{\left|\boldsymbol{E}^i_0\right|^2} \\ &= \frac{\left|\mathbf{S}^+ \cdot \boldsymbol{E}^i_{0xy} + \mathbf{G}^+_{00} \cdot \boldsymbol{E}_{xy}|_U(\boldsymbol{k}_{00})\right|^2}{\left|\boldsymbol{E}^i_0\right|^2} = \frac{\left|\mathbf{T}_{00} \cdot \boldsymbol{E}^i_{0xy}\right|^2}{\left|\boldsymbol{E}^i_0\right|^2}, \qquad \text{no grating lobes} \end{aligned}$$

8 Numerical examples

In this section, we illustrate the algorithms presented above. The code is verified by comparisons with the Periodic Method of Moment program (PMM) [14] and with scattering matrix formulation [4, 5, 18].

In Figure 4, we depict the reflection and transmission coefficients for a skewed array of dipoles. This geometry is not intended to be useful in applications, but it is used to verify the implementation of the present method. The results are compared with the Periodic Method of Moment program (PMM) [14]. The agreement is excellent.

In Figure 5, the reflection coefficient for a gangbuster FSS type 3 [9] is shown. For parallel polarization, the electric field is parallel to the linear dipoles. Thus, for parallel polarization, the elements will resonate when the length of the dipole arms is about $\lambda/2$, where λ is the wavelength in the substrate. However, for orthogonal polarization, the electric field is orthogonal to the dipole arms, which means that the reflected field is scattered from the substrate alone. The first resonance of the substrate occurs when the thickness of the substrate is $\lambda_0/(2\sqrt{\epsilon - \sin^2\theta})$, where λ_0 is the wavelength in vacuum. For the data in Figure 5, this resonance occurs at approximately 6.1 GHz. In the figure, the present method is compared to the

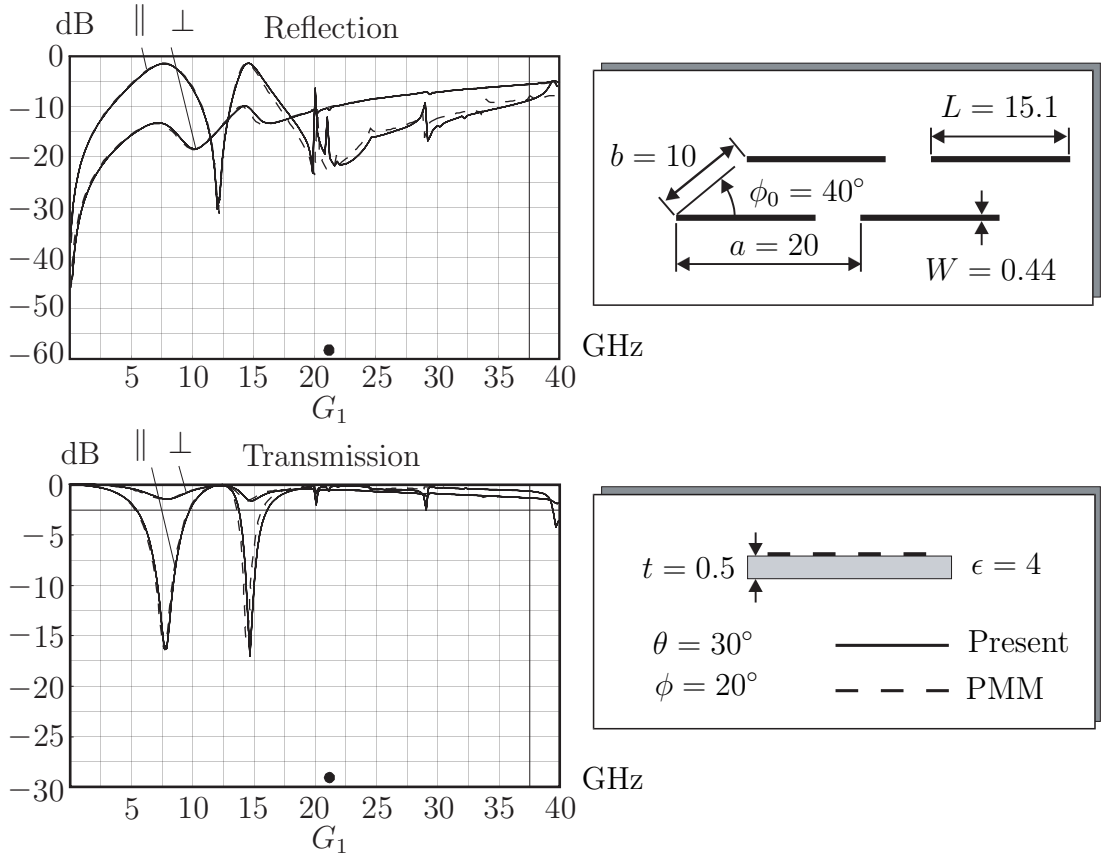

Figure 4: The reflection and transmission coefficients for a skewed array of dipoles. The onset of the grating lobes is at 21.3 GHz. The dashed curves are computed by the Periodic Method of Moment program (PMM) with 3 piecewise sinusoidal modes taken into account. The solid curves are computed by the present method using 3 basis functions, namely 2 even (cosine) and 1 odd (sine) dipole basis function. Moreover, $(2 \times 5 + 1)^2$ Floquet modes are included.

scattering matrix method [4, 5, 18]. Both methods agree very well. However, the computation times differ substantially. A rough estimate of the difference in evaluation time between the computations shown in Figure 5 is that the present method is more than 200 times faster than the traditional scattering matrix method. More numerical experiments have to be made in order to see whether this reduction of computation time is true in general.

9 Conclusions

A new powerful method to compute the scattering properties in planar geometries with planar metal inclusions has been presented in this paper. The method employs the propagator technique [17], which is thoroughly discussed. The main advantage

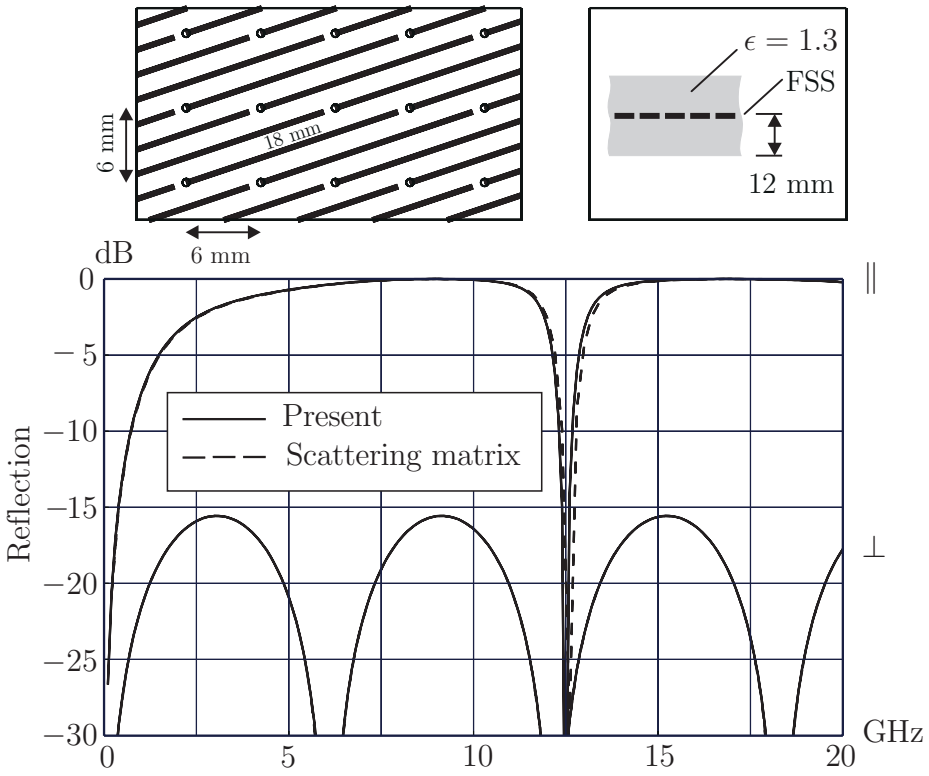

Figure 5: The reflection coefficient for a gangbuster FSS type 3 [9]. The length of the dipole arms is 18 mm, while the width is 0.5 mm. The plane of incidence is parallel to the dipoles (*i.e.*, $\phi = 18.4°$), and the angle of incidence is $\theta = 30°$. The solid curve is computed with the present method using 3 basis functions and $(2 \times 5 + 1)^2$ Floquet modes. The dashed curve is computed by the scattering matrix approach [4, 5, 18] using scattering matrices of the size $2(2 \times N + 1)^2 \times 2(2 \times N + 1)^2$, with $N = 4$, *i.e.*, interaction modes up to order $N = 4$ are included.

with this method is that all effects of the complex interaction between the metal inclusions and the materials are included in the formulation. This type of geometry can also be analyzed with other methods, *e.g.*, the Green's function method [11], but the present method is superior in its systematic structure. As a consequence, there is no need to identify the numerous reflection and transmission dyadics of the individual bianisotropic slabs that support the metal inclusions and, moreover, no cascade procedure is needed.

Several extensions of the method presented in this paper are possible. The Green's dyadic for a geometry depicted in Figure 1 is straightforward to compute and these results are reported elsewhere. Other boundary condition, such as the perfectly conducting ground plane is treated in [12]. The propagators are also an excellent instrument for the analysis of possible surface waves in the slab. This analysis is postponed to a separate paper, see also [12].

Acknowledgement

The work reported in this paper is supported by grants from the Swedish Defence Materiel Administration (FMV) and by the Swedish Foundation for Strategic Research (SSF), which are gratefully acknowledged.

Appendix A Periodic function

If f is a doubly periodic function in $\boldsymbol{\rho} \in \mathbb{R}^2$ with unit cell $U = \{\boldsymbol{a}s+\boldsymbol{b}t \colon 0 \leq s,t \leq 1\}$, defined by the linearly independent vectors $\boldsymbol{a} \in \mathbb{R}^2$ and $\boldsymbol{b} \in \mathbb{R}^2$, then

$$\begin{cases} f(\boldsymbol{\rho}+\boldsymbol{a}) = f(\boldsymbol{\rho}) & (\boldsymbol{\rho} \in \mathbb{R}^2), \\ f(\boldsymbol{\rho}+\boldsymbol{b}) = f(\boldsymbol{\rho}) & (\boldsymbol{\rho} \in \mathbb{R}^2). \end{cases}$$

Clearly, if $\boldsymbol{q} \in \mathbb{R}^2$, then the complex exponential

$$f(\boldsymbol{q},\boldsymbol{\rho}) = \exp{(i\boldsymbol{q}\cdot\boldsymbol{\rho})}, \qquad \boldsymbol{\rho} \in \mathbb{R}^2$$

satisfies these conditions if and only if

$$\begin{cases} \boldsymbol{q}\cdot\boldsymbol{a} = m2\pi \\ \boldsymbol{q}\cdot\boldsymbol{b} = n2\pi \end{cases} \qquad m,n \in \mathbb{Z}$$

Consequently, if f can be expanded in a Fourier series, then

$$f(\boldsymbol{\rho}) = \sum_{m,n=-\infty}^{\infty} f_{mn} \exp{(i\boldsymbol{q}_{mn}\cdot\boldsymbol{\rho})}$$

where the reciprocal lattice is defined by

$$\boldsymbol{q}_{mn} = 2\pi\left(-m\frac{\hat{\boldsymbol{z}}\times\boldsymbol{b}}{\hat{\boldsymbol{z}}\cdot(\boldsymbol{a}\times\boldsymbol{b})} + n\frac{\hat{\boldsymbol{z}}\times\boldsymbol{a}}{\hat{\boldsymbol{z}}\cdot(\boldsymbol{a}\times\boldsymbol{b})}\right)$$

and $\hat{\boldsymbol{z}}\cdot(\boldsymbol{a}\times\boldsymbol{b})$ is the area of the unit cell (with sign). Due to the integral

$$\begin{aligned} \iint_U \exp{(i\boldsymbol{q}_{mn}\cdot\boldsymbol{\rho})}dxdy =& |\hat{\boldsymbol{z}}\cdot(\boldsymbol{a}\times\boldsymbol{b})| \iint_{0\leq s,t\leq 1} \exp{(2\pi i\,(ms+nt))}dsdt \\ =& |\hat{\boldsymbol{z}}\cdot(\boldsymbol{a}\times\boldsymbol{b})|\delta_{m0}\delta_{n0} \end{aligned}$$

where the Jacobian $|\hat{\boldsymbol{z}}\cdot(\boldsymbol{a}\times\boldsymbol{b})|$ equals the area of the unit cell U, the Fourier coefficients of f are

$$f_{mn} = \frac{1}{|\hat{\boldsymbol{z}}\cdot(\boldsymbol{a}\times\boldsymbol{b})|}\iint_U f(\boldsymbol{\rho})\exp{(-i\boldsymbol{q}_{mn}\cdot\boldsymbol{\rho})}dxdy. \tag{A.1}$$

Moreover, if g is another doubly periodic function in $\boldsymbol{\rho} \in \mathbb{R}^2$ with unit cell U and Fourier coefficients g_{mn}, a similar calculation gives Parseval's formula:

$$\frac{1}{|\hat{\boldsymbol{z}}\cdot(\boldsymbol{a}\times\boldsymbol{b})|}\iint_U f^*(\boldsymbol{\rho})g(\boldsymbol{\rho})dxdy = \sum_{m,n=-\infty}^{\infty} f^*_{mn}g_{mn}. \tag{A.2}$$

References

[1] J. D. Bjorken and S. D. Drell. *Relativistic Quantum Mechanics*. McGraw-Hill, New York, 1964.

[2] W. C. Chew. *Waves and fields in inhomogeneous media*. IEEE Press, Piscataway, NJ, 1995.

[3] R. E. Collin. *Foundations for Microwave Engineering*. McGraw-Hill, New York, second edition, 1992.

[4] T. A. Cwik and R. Mittra. The cascade connection of planar periodic surfaces and lossy dielectric layers to form an arbitrary periodic screen. *IEEE Trans. Antennas Propagat.*, **35**(12), 1397–1405, December 1987.

[5] T. A. Cwik and R. Mittra. Correction to "The cascade connection of planar periodic surfaces and lossy dielectric layers to form an arbitrary periodic screen". *IEEE Trans. Antennas Propagat.*, **36**(9), 1335, September 1988.

[6] L. B. Felsen and N. Marcuvitz. *Radiation and scattering of waves*. Prentice-Hall, Inc., Englewood Cliffs, New Jersey, first edition, 1973.

[7] A. Ishimaru. *Electromagnetic Wave Propagation, Radiation, and Scattering*. Prentice-Hall, Inc., Englewood Cliffs, New Jersey, 1991.

[8] J. A. Kong. *Electromagnetic Wave Theory*. John Wiley & Sons, New York, 1986.

[9] T. W. Kornbau. *Analysis of periodic arrays of rotated linear dipoles, rotated crossed dipoles, and of biplanar dipole arrays in dielectric*. PhD thesis, The ElectroScience Laboratory, The Ohio State University, Department of Electrical Engineering, Columbus, Ohio 43212, USA, 1984.

[10] R. Kress. *Linear Integral Equations*. Springer-Verlag, Berlin Heidelberg, 1989.

[11] G. Kristensson, M. Åkerberg, and S. Poulsen. Scattering from a frequency selective surface supported by a bianisotropic substrate. Technical Report LUTEDX/(TEAT-7085)/1–28/(2000), Lund Institute of Technology, Department of Applied Electronics, Electromagnetic Theory, P.O. Box 118, S-211 00 Lund, Sweden, 2000.

[12] G. Kristensson, P. Waller, and A. Derneryd. Radiation efficiency and surface waves for patch antennas on inhomogeneous substrates. Technical Report LUTEDX/(TEAT-7100)/1–45/(2001), Lund Institute of Technology, Department of Electroscience, P.O. Box 118, S-211 00 Lund, Sweden, 2001.

[13] I. V. Lindell, A. H. Sihvola, S. A. Tretyakov, and A. J. Viitanen. *Electromagnetic Waves in Chiral and Bi-isotropic Media*. Artech House, Boston, London, 1994.

[14] B. Munk. *Frequency Selective Surfaces: Theory and Design*. John Wiley & Sons, New York, 2000.

[15] S. Poulsen. Scattering from frequency selective surfaces: A continuity condition for entire domain basis functions and an improved set of basis functions for crossed dipole. *IEE Proc.-H Microwaves, Antennas and Propagation*, **146**(3), 234–240, 1999.

[16] D. M. Pozar. *Microwave Engineering*. John Wiley & Sons, New York, 1998.

[17] S. Rikte, G. Kristensson, and M. Andersson. Propagation in bianisotropic media—reflection and transmission. *IEE Proc.-H Microwaves, Antennas and Propagation*, **148**(1), 29–36, 2001.

[18] N. Shuley. Analytical and numerical study of two-dimensional multilayer structures for use as dichroic surfaces. Technical Report TR 8404, Division of Network Theory, Chalmers University of Technology, 1984.

[19] J. R. Wait. *Electromagnetic Waves in Stratified Media*. Pergamon, New York, second edition, 1970.